Title: Insulin receptors in pancreatic acinar cells contribute to *Kras*^{G12D}-driven cancer initiation in the context of diet-induced obesity

Authors: Anni M.Y. Zhang[1], Yi Han Xia[1], Ken H. Chu[1], Titine J.J. Ruiter[1], Jenny C.C. Yang[1], Jeffrey S.H. Lin[1], Nan Chen[1], Justin Chhuor[1], Shilpa Patil[1], Haoning Howard Cen[1], Elizabeth J. Rideout[1], Vincent R. Richard[3], David F. Schaeffer[2], Rene P. Zahedi[3,4,5], Christoph H. Borchers[3,6], James D. Johnson[1] *, Janel L. Kopp[1] *

Affiliations: [1]Department of Cellular and Physiological Sciences, Life Sciences Institute, University of British Columbia, Vancouver, Canada; [2]Department of Pathology and Laboratory and Medicine, University of British Columbia, Vancouver, Canada; [3]Segal Cancer Proteomics Centre, Lady Davis Institute, Jewish General Hospital, McGill University, Montreal, Canada. [4]Department of Internal Medicine, University of Manitoba, Winnipeg, Canada. [5]Manitoba Centre for Proteomics and Systems Biology, Winnipeg, Canada. [6]Gerald Bronfman Department of Oncology, Jewish General Hospital, McGill University, Montreal, Canada.

***Correspondence**: janel.kopp@ubc.ca or james.d.johnson@ubc.ca

Keywords: pancreatic ductal adenocarcinoma, PanIN, hyperinsulinemia, obesity, insulin resistance

Abstract word count: 208
Body word count: 5746
Reference count: 69
Main figure count: 5

Funding: The project was supported by CIHR grants to E.J.R (PJT-153072), J.L.K. (MOP-142216 and PJT-162239) and J.D.J. (PJT - 168854) and by a Lustgarten Foundation Therapeutics Focused Research Program grant to J.D.J. and J.L.K. A.M.Y.Z was supported by Frederick Banting and Charles Best Canada Graduate Scholarships and a Four-Year Fellowship from the University of British Columbia. J.L.K was supported by a CIHR New Investigator Award (Msh-147794) and the MSFHR Scholar Award (18309). E.J.R was supported by the CIHR Sex and Gender Chair Program (GSA-171465) and the MSFHR Scholar Award (16876). C.H.B is grateful to Genome Canada for financial support through the Genomics Technology Platform (GTP: 264PRO) and the Quebec Cancer Consortium, Ministère de l'Économie et de l'Innovation, Quebec. C.H.B is also grateful for support from the Segal McGill Chair in Molecular Oncology at McGill University (Montreal, Quebec, Canada), and for support from the Warren Y. Soper Charitable Trust and the Alvin Segal Family Foundation to the Jewish General Hospital (Montreal, Quebec, Canada).

Author Contributions: A.M.Y.Z designed, managed, and conducted the project including acquiring and interpreting the majority of the data and she wrote the manuscript. Y.X performed the proteomics and phospho-proteomics analyses. K.H.C. and J.C. provided technical assistance with pancreas sectioning and staining (Alcian blue, H&E, CK19, or GFP). J.C.C.Y provided technical assistance with dissection and CK19 staining. T.J.J.R and J.S.H.L. provided technical assistance with dissection and genotyping. N.C. analysed staining (Sirius red). S.P. assisted on dissection and sample preparation. H.H.C. assisted with proteomics sample preparation and proteomics analyses. E.J.R. evaluated the manuscript and helped with interpretation of the data in a sex-specific manner. V.R.R., R.P.Z. and C.H.B. co-designed and conducted proteomic analyses. D.F.S. provided histopathology analysis and expertise. C.H.B., J.L.K., and J.D.J. supervised the project, obtained funding, interpreted the data, and edited the manuscript. J.L.K. is the guarantor of this work.

Acknowledgements: The authors thank members from Johnson and Kopp labs for discussions. We thank Chris Wright (Vanderbilt, USA) for the *Ptf1a*^{CreER} mice.

Conflict of interest: The authors report no relevant conflicts of interest.

Availability of data and materials: All data generated and analyzed in this study is included within the article, additional files, or is available from the corresponding author on request.

Abstract

The rising incidence of pancreatic cancer is largely driven by increased prevalence of obesity and type 2 diabetes (T2D). Hyperinsulinemia is a cardinal feature of obesity and T2D, and is associated with increased cancer incidence and mortality. Genetic reduction of insulin production suppresses formation of pancreatic intraepithelial neoplasia (PanIN) pre-cancerous lesions in mice with mutant *Kras*. However, it remained unclear whether hyperinsulinemia exerts its tumorigenic effects directly on the cells that give rise to PanINs or indirectly on the tumor microenvironment. Here, we tested whether diet-induced hyperinsulinemia contributes to pancreatic cancer directly through insulin receptor (Insr) signaling in *Kras*^{G12D}-expressing pancreatic acinar cells. Loss of insulin receptors in wild-type or Kras^{G12D}-expressing acinar cells did not significantly influence fasting glucose or insulin. Strikingly, mice lacking *Insr* in Kras^{G12D}-expressing acinar cells and their progeny had a significant reduction in PanIN plus tumor area in males (2.7-fold) and females (5.3-fold) compared to control mice. Mechanistically, proteome analyses implicated a reduction in digestive enzymes among altered protein networks in mice protected from PanINs, and together with phospho-proteome analysis, linked the spliceosome, ribosome, and secretory pathway to insulin signaling in context of pancreatic cancer initiation. Collectively, these data demonstrate that insulin receptor signaling in acinar cells promotes PanIN initiation in the context of obesity.

Introduction

The 5-year survival rate of pancreatic ductal adenocarcinoma (PDAC) is less than 10% and it is projected to become the 2nd leading cause of cancer death by 2030[1]. Chronic pancreatitis, family history, smoking, obesity, and T2D are risk factors for pancreatic cancer[2]. Obesity and T2D are usually accompanied by hyperinsulinemia, hyperglycemia, increased inflammation, and dyslipidemia, which have all been proposed as underlying factors that drive the increased PDAC morbidity and mortality in this patient population[3,4]. Epidemiological studies consistently shown that hyperinsulinemia is associated with increased risk of developing PDAC and poorer survival[5,6]. Complementing human observations, our *in vivo* animal experiments demonstrated that endogenous hyperinsulinemia causally contributes to PDAC development[7,8]. Notably, stimulation of PanIN development by hyperinsulinemia is independent of hyperglycemia[7,8]. Single-cell analysis revealed that hyperinsulinemia altered gene expression in multiple cell types in the PanIN microenvironment[8], leaving open the question of whether the protective effects of reduced insulin production were direct on the tumor precursor cells or whether they were mediated indirectly by local immune cells, local fibroblasts, and/or via distant effects on adiposity[9-11]. Consistent with a direct effect on the epithelium, insulin stimulates proliferation in the PANC-1 and HPDE cell lines *in vitro*[12], but this does not provide information on the initiation of PDAC.

Insulin/IGF signaling, which includes KRAS/MAPK/ERK or PI3K/AKT/mTOR cascades, is prominent in human and animal pancreatic cancer. *KRAS* mutations are detected in ~95% of PDAC clinical cases and are sufficient to induce PanIN pre-cancerous lesions and rare tumours in mice[13]. *PIK3CA*, is mutated in 3-5% of PDAC patients[14,15] and is also sufficient to initiate PDAC in mice[16]. Additionally, *Pik3ca* silencing was protective in *Pdx1*-Cre;*Kras*$^{LSL\text{-}G12D}$;*Trp53*$^{LSL\text{-}R172H}$ mice[17]. Strategies that systemically reduce signaling downstream of Insr/Igf1r can suppress PDAC[16,18], but they do not distinguish between the roles for insulin, IGFs, or other upstream growth factors. Despite indirect evidence for an important role of insulin/IGF signaling in this and other cancers, a cell autonomous and causal role for the insulin receptor has not been demonstrated for any cancer. Insulin receptor protein is upregulated in some breast, prostate, and liver cancers[19-21], but its role in the pancreas remains enigmatic.

In this study, we tested the hypothesis that hyperinsulinemia-induced enhancement of PDAC initiation is mediated through direct insulin receptor signaling in pancreatic acinar cells. We found a significant reduction in PanIN and tumor development in mice lacking acinar cell *Insr*, in the context of diet-induced obesity. These findings suggest that hyperinsulinemia directly contributes to pancreatic cancer initiation through Insr signaling.

Methods

Mice

All animal experiments were conducted at the University of British Columbia with approval of the University of British Columbia Animal Care Committee in accordance with Canadian Council for Animal Care guidelines. All alleles have been described previously[22-27]. *Kras*$^{LSL\text{-}G12D/w}$ (#008179), *Insr*$^{f/f}$ (#006955), and nuclear TdTomato-to-nuclear EGFP (nTnG) mice (#023035) were purchased from Jackson Labs (Bar Harbour, USA). *Ptf1a*$^{CreER/w}$ mice (C57BL/6) were a gift from Chris Wright (Vanderbilt, USA). Mice were maintained on C57BL/6 genetic background and housed at the University of British Columbia Modified Barrier Facility which was temperature-controlled and specific pathogen-free. They were kept on a 12:12 hr light: dark cycle with food and drinking water *ad libitum*. To generate genetic background-matched *Ptf1a*$^{CreER/w}$;*Kras*$^{LSL\text{-}G12D/w}$;*Insr*$^{w/w}$;nTnG, *Ptf1a*$^{CreER/w}$;*Kras*$^{LSL\text{-}G12D/w}$;*Insr*$^{w/f}$;nTnG, and *Ptf1a*$^{CreER/w}$;*Kras*$^{LSL\text{-}G12D/w}$;*Insr*$^{f/f}$;nTnG mice, *Ptf1a*$^{CreER/w}$;*Kras*$^{LSL\text{-}G12D/w}$;*Insr*$^{w/f}$;nTnG mice were bred with *Insr*$^{w/f}$ mice. After weaning (3 weeks), the resulting litters were fed with high fat diet (HFD), and at 4 weeks of age, recombination was induced over three consecutive days by subcutaneous injections of tamoxifen in corn oil (20 mg/mL) of 5 mg tamoxifen/40 g body mass. One cohort of mice was euthanized at 10 months of age for histopathology analyses and the whole pancreas was used for histopathology analyses. Another cohort of mice was euthanized at 12 weeks of age. For mice euthanized at 12 weeks, each pancreas was cut into three pieces roughly based on the pancreas anatomical structure: head, body, and tail. The body piece was used for histopathological analyses, while the other pieces were snap frozen in liquid nitrogen and kept at -80°C. The head piece was processed for proteomics and phospho-proteomics analyses (see below).

Assessment of glucose homeostasis

Mouse body weight and fasting blood glucose levels were measured every 4 weeks and fasting insulin were measured every 3 months. Before the measurements, mice were fasted for 4 hours in clean and fresh cages during the light period. One drop of blood was collected from each mouse's saphenous vein and a Lifescan OneTouch Ultra Mini glucometer was used to measure the fasting blood glucose levels. About 30 µl of blood was collected with a heparinized microhematocrit capillary tube (Fisher Scientific, 22-362566, Waltham, MA, USA) for measuring fasting insulin levels. The collected blood was centrifuged at 10,000 rpm for 10 minutes to collect the blood serum. Then the blood serum was kept at -20°C until used to measure the fasting insulin levels with insulin ELISA (80-INSMSU-E10; ALPCO Diagnostics, Salem, NH).

Histopathological, morphological, and immunohistochemical analyses

Pancreata were fixed in 4% paraformaldehyde for 24 hours followed by paraffin embedding. Mouse pancreata were sectioned then stained with hematoxylin and eosin (H&E), and Alcian blue as

previously described[7,8,28]. The stained slides were scanned with a 20x objective using a 3DHISTECH Panoramic MIDI (Quorum Technologies Inc. Guelph, Canada) slide scanner. Histopathological analyses were conducted in a de-identified manner and verified separately by J.L.K and D.F.S. All histopathological analyses were performed on one of the stained sections that displayed the maximal pancreatic cross-sectional area unless otherwise stated. Every gland with a lumen was categorized as normal, ADM, PanIN, or neoplasia, and glands representing more than one of these categories were scored based on their highest-grade feature. The total pancreatic area, PanIN plus tumor area, PanIN area, and normal acinar cell area were measured as previously described[7,8]. Briefly, the total pancreatic area, PanIN plus tumor area, PanIN area, normal acinar cell area was determined by masking all pancreatic tissue, selective masking of the PanIN plus tumor area, selective masking of the only PanIN area, and selective masking of the normal acinar cell area by Adobe Photoshop, respectively. Pixels for the total pancreatic area or each histological feature were measured by ImageJ and this was used to calculate the percentage area occupied by each histological feature. For Alcian blue positive area, Adobe Photoshop 2020 Black & White function was used to highlight the blue area (red filter). The total pixels for pancreas or Alcian blue positive area were counted using ImageJ.

Immunohistochemical (IHC) staining was performed according to published standard protocols[8,28]. Primary antibodies were rabbit anti-cytokeratin 19 (CK19) (Abcam, ab133496, 1:1000) and goat anti-GFP (Abcam, ab6673, 1:200). Secondary antibodies were biotin-conjugated donkey anti-rabbit (Jackson ImmunoResearch Laboratories, Inc., 711-065-152, 1:500) and biotin-conjugated rat anti-goat (Vector Laboratories, MP-7404, 1:2). IHC slides were scanned with a 20x objective using a 3DHISTECH Panoramic MIDI slide scanner. CK19 positive area was measured with Adobe Photoshop 2020 using the Black & White function to filter and highlight the brown area (blue filter), which was then taken as a percent of pixels in the pancreatic section.

Proteomics analyses

The whole head of pancreata collected from female mice at 12 weeks of age (*Ptf1a*^{CreER};*Kras*$^{LSL-G12D}$;*Insr*$^{w/w}$;nTnG (n=3), *Ptf1a*^{CreER};*Kras*$^{LSL-G12D}$;*Insr*$^{w/f}$;nTnG (n=6), *Ptf1a*^{CreER};*Kras*$^{LSL-G12D}$;*Insr*$^{f/f}$;nTnG (n=6), *Ptf1a*^{CreER};*Insr*$^{w/w}$;nTnG (n=3), and *Ptf1a*^{CreER};*Insr*$^{f/f}$;nTnG (n=2) mice) were frozen and used for (phospho)proteomic analyses. The frozen sample was ground into powder in a liquid nitrogen-cooled mortar and pestle and kept on dry ice until mass-spec analysis. Proteins were extracted from cryopulverized tumors in a buffer containing 5% sodium dodecyl sulfate (SDS) and 100 mM TRIS pH 7.8 supplemented with PhosStop phosphatase inhibitor cocktail (Roche). The protein concentration of the lysate was determined using bicinchoninic acid assay (BCA) (Thermo Fisher Scientific), and protein disulfide bonds were reduced and free Cysteines alkylated with 20 mM tris(2-carboxyethyl)phosphine (TCEP) and 30 mM iodoacetamide, respectively. 250 µg of total protein was used for proteolytic digestion using S-TRAP Mini columns (Protifi LLC, Huntington NY)[29]. Resultant

tryptic peptides were then vacuum concentrated and desalted using Oasis HLB SPE cartridges (Waters). Peptides were vacuum concentrated and reconstituted in 0.1% trifluoro acetic acid (TFA), and 10% of the total sample was reserved for measurement of the total proteome. The remaining 90% of the sample was diluted in 80% acetonitrile with 0.1% TFA for automated phosphopeptide enrichment using AssayMap Fe-NTA (III) immobilized metal affinity chromatography (IMAC) cartridges and a Bravo liquid handling system using the phosphopeptide enrichment v 2.1 application (Agilent).

LC-MS/MS acquisition and data analysis

Samples for both total proteome and phosphoproteome were analyzed by data dependent acquisition (DDA) using an Easy-nLC 1200 and Q Exactive Plus (both Thermo Fisher Scientific). Samples were first loaded onto a precolumn (Acclaim PepMap 100 C18, 3 µm particle size, 75 µm inner diameter x 2 cm) in 0.1% formic acid (buffer A), and gradient elution was performed using a 100-min method from 3 to 40% buffer B (84% acetonitrile, 0.1% formic acid) on the analytical column (Acclaim PepMap 100 C18, 2 µm particle size, 75 µm inner diameter x 25 cm) at a flow rate of 300 nL/min. MS scans were acquired between 350-1,500 m/z at a resolution of 70,000, with an automatic gain control (AGC) target of 1 x 10e610E6 ions and a maximum injection time of 50 ms. The top 15 precursor ions with charge states +2, +, +3, and +4 were isolated with a window of 1.2 m/z, an AGC target of 2 x 10e410E4 and a maximum injection time of 64 ms and fragmented using a normalized collision energy (NCE) of 28. MS/MS were acquired at a resolution of 17,500 and the dynamic exclusion was set to 30 s. DDA MS raw data was processed with Proteome Discoverer 2.5 (Thermo Scientific) and searched using Sequest HT against the mouse reference proteome FASTA database from Uniprot (downloaded October 1st 2021; 17,054 forward sequences). The enzyme specificity was set to trypsin with a maximum of 2 missed cleavages. Carbamidomethylation of cysteine was set as a fixed modification and oxidation of methionine, as well as phosphorylation of serine, threonine, and tyrosine as variable modifications. The precursor ion mass tolerance was set to 10 parts per million, and the product ion mass tolerance was set to 0.02 Da. Percolator was used to assess posterior error probabilities and the data was filtered using a false discovery rate (FDR) of <1% on peptide and protein level. The Minora node of Proteome Discoverer was used for label free quantitation.

Statistical analyses and data visualization

Animals were excluded from the histopathological analyses if they were found dead or if nTnG recombination efficiency (% acinar cells or PanIN cells labeled with GFP) was lower than 20%. Statistical analyses were conducted with GraphPad Prism 9.3.0. The Shapiro-Wilk test was used to assess data normality. One-way ANOVA was performed unless otherwise stated. Mixed-effect analyses were run for glucose homeostasis data (mouse body weight, fasting glucose level, and fasting insulin level). When comparing the histopathological measurements between male and female

mice from the same genotype, a two-tailed student's t-test was run for normally distributed data and a Mann-Whitney test was performed for non-normally distributed data. Statistical parameters, including the exact value of sample size n (animal number), precision measures and dispersion (mean ± SEM), and statistical significance levels, are reported in the figures and figure legends. A p-value <0.05 was considered as significant. In figures, asterisks denote statistical significance (*p<0.05, **p<0.01, ***p<0.001, and ****p<0.0001).

For total proteomics data, normalization, imputation, and differential expression analyses were performed on the protein abundances using Proteome Discoverer. Differential expression analysis used background-based t-tests with p-values adjusted using Benjamini-Hochberg correction. The proteins were filtered for significant comparisons (Adj. p<0.05), and heatmaps were created with resultant protein lists. We also applied k-means clustering and extracted clusters with patterns of interest[30]. From this heatmap, a class of specific secreted proteins were identified and values for all samples were plotted in a heatmap and sorted with hierarchical clustering. We used STRING (v11) to generate an edge table with differentially expressed total proteins (Adj. p<0.05) with an absolute $\log_2$(Fold Change) cut-off of 2.5 in *Ptf1a*^{CreER};*Kras*$^{LSL\text{-}G12D}$;*Insr*$^{w/w}$;nTnG compared to *Ptf1a*^{CreER};*Kras*$^{LSL\text{-}G12D}$;*Insr*$^{f/f}$;nTnG. Protein-protein relationships were only included if they involved experimental evidence or interactions annotated in other databases[31]. Cytoscape (v3.9.1) was used to visualize the network[32], with background images created with BioRender.com.

Phospho-proteomics data were analyzed two ways. In the first approach, we only used phospho-peptides with measurements made in a minimum of 2/3 of all the samples and at least one sample per group. We imputed missing phospho-protein values in samples before normalization and statistical analysis using the same process as the total proteomics, allowing a broader assessment of the phospho-protein landscape. These were plotted using volcano plots and against the corresponding proteins in the total protein data set with calculated $\log_2$(Fold Change) of the median. In the second approach, we aggregated the abundances of each sample for each phospho-site detected, and normalized each of the detected phospho-sites to the total abundance of the corresponding protein. We only included phospho-sites where every sample had an experimentally measured total protein value. The second method used differential expression analysis performed using the R package limma on the *Ptf1a*^{CreER};*Kras*$^{LSL\text{-}G12D}$;*Insr*$^{w/w}$;nTnG vs *Ptf1a*^{CreER};*Kras*$^{LSL\text{-}G12D}$;*Insr*$^{f/f}$;nTnG comparison[33]. The top differentially abundant phospho-sites (sorted by Adj. p-value) were plotted as a heatmap and sorted with hierarchical clustering[30]. Phosphosite (www.phosphosite.org) was used to determine upstream activators, cellular location, and function of each protein, as well as the specific kinases of the detected phospho-sites (if known). STRING was used to identify proteins that physically interact with each other[31].

Results

Effects of acinar cell-specific *Insr* loss on body weight and glucose homeostasis

We generated mouse models in which *Kras*^{G12D} expression and loss of *Insr* were both induced in acinar cells to test whether hyperinsulinemia drives pancreatic cancer development via Insr signaling cell autonomously. Our cohorts contained mice with full insulin receptor signaling, *Ptf1a*^{CreER};*Kras*$^{LSL-G12D}$;*Insr*$^{w/w}$;nTnG (PK-*Insr*$^{w/w}$); mice with reduced insulin receptor signaling, *Ptf1a*^{CreER};*Kras*$^{LSL-G12D}$;*Insr*$^{w/f}$;nTnG (PK-*Insr*$^{w/f}$); or mice without insulin receptor signaling, *Ptf1a*^{CreER};*Kras*$^{LSL-G12D}$;*Insr*$^{f/f}$;nTnG (PK-*Insr*$^{f/f}$) mice in Kras^{G12D}-expressing acinar cells (Fig. 1A). We also generated *Ptf1a*^{CreER};*Insr*$^{w/w}$;nTnG or *Ptf1a*^{CreER};*Insr*$^{f/f}$;nTnG mice that do not have the *Kras*$^{LSL-G12D}$ allele to assess the baseline roles of acinar cell *Insr* (Extended Data. 1A). All mice were fed with HFD after 3 weeks of age to sustain hyperinsulinemia. Multiple studies have shown that HFD accelerates PanIN and PDAC development[34,35]. Tamoxifen was injected at 4 weeks of age to induce recombination and expression of *Kras*^{G12D} and a Cre-dependent nTnG allele[36], as well as recombination of the *Insr*^{flox} alleles, specifically in acinar cells (Fig. 1B). *Insr* loss did not significantly affect body weight in male or female mice in the context of mutant *Kras* (Fig. 1C-D). We observed a small, but significant, reduction in body weight in female *Ptf1a*^{CreER};*Insr*$^{f/f}$;nTnG mice compared to *Ptf1a*^{CreER};*Insr*$^{w/w}$;nTnG mice (Extended Data. 1C). Fasting glucose was also similar between groups (Fig. 1E-F and Extended Data. 1D-E). HFD induced similar hyperinsulinemia in all groups (Fig. 1G-H and Extended Data. 1F-G), well above the expected fasting insulin levels of C57Bl6J mice on a chow diet (138 +/- 24 pM)[37]. Thus, our model enabled us to test the role of acinar cell *Insr* in the context of intact hyperinsulinemia and normoglycemia that normally characterize the obese state.

Loss of *Insr* in *Kras*^{G12D}-expressing acinar cells reduced PanIN development

Our previous studies showed that hyperinsulinemia promotes the initiation of pancreatic precursor lesions[7,8]. To examine whether loss of *Insr* suppresses the development of lesions from acinar cells, we generated a cohort of 9-12 mice for each sex and genotype and planned to assess lesions at ~1 year of age. Previous studies of the effects of HFD on PDAC development suggested that male mice formed lesions faster than female mice[35]. Indeed, we observed that half the *Insr*$^{w/w}$ male mice reached humane endpoint earlier than we had expected (Extended Data. 2A) based on our previous work[7,8]. This suggested that HFD promoted tumor development in mice with full insulin gene dosage earlier than in mice with reduced insulin[7,8]. We revised our endpoint to ~10 months of age (43.5 weeks) to quantify PanIN and tumor formation at the same age. At necropsy and by histology we found that PDAC formation in females was Insr dosage-dependent, while in male mice tumor formation appeared to be more prevalent in PK-*Insr*$^{f/f}$ compared to PK-*Insr*$^{w/w}$ mice (50% vs 20%, respectively) (Fig. 2A-B, Extended Data 2A). The latter observation, however, is likely due faster progression of disease in

male mice, such that the tissues from many males were not available to be included in our histopathological analyses at 43.5 weeks of age. Altogether these results indicate that male PK-*Insr*$^{w/w}$ mice tended to reach humane endpoint earlier than PK-*Insr*$^{f/f}$ mice, this is likely due to earlier tumor formation and/or pancreatic insufficiency from the near total disruption of the normal parenchyma (Fig. 2A-B, Extended Data 2A). In most female mice of all genotypes, however, some normal parenchyma remained, suggesting that the extent of disruption was different compared to males and that at 10 months of age, female mice had yet not reached the maximal level of lesion formation. This suggested that the timing and/or extent of lesion formation between male and female mice in the context of HFD may differ. In summary, these data strongly suggested that limiting insulin/Insr activity in acinar cells in mice fed HFD reduced the latency of PDAC formation in a dose-dependent manner in both sexes.

We next quantified the extent of the PanIN lesions present at 43.5 weeks of age to assess the extent of disease present in the presence and absence of Insr. Prior to PanIN quantification between groups, we stained for nuclear GFP from the nTnG lineage reporter allele[36] in all pancreata. As expected, most acinar cells and PanIN lesions were GFP positive (Extended Data 3A-B). Rare mice with a GFP labeling efficiency below 20% were excluded from further analysis. Pancreata from *Ptf1a*^{CreER};*Insr*$^{w/w}$;nTnG and *Ptf1a*^{CreER};*Insr*$^{f/f}$;nTnG mice had wide-spread GFP in acinar cells (Extended Data 4A-B), consistent with their *Kras* wild-type genotype. In contrast, pancreata from male and female PK-*Insr*$^{w/w}$, PK-*Insr*$^{w/f}$, and PK-*Insr*$^{f/f}$ mice all contained ductal lesions with histological characteristics of metaplastic ducts, including ADM, low-grade and high-grade PanIN, and sometimes PDAC (see above) (Figure 2A-B). When we quantified the PanIN and/or tumor area, we found that loss of *Insr* from Kras^{G12D}-expressing acinar cells reduced the area of PanINs plus tumors (2.9-fold and 5.3-fold reduction for PK-*Insr*$^{f/f}$ male and female mice, respectively, in comparison to PK-*Insr*$^{w/w}$ mice), or PanIN alone, in a dose dependent manner in males and females (Fig. 2C-F). Consistent with this histological-based quantification, measuring the pancreatic area containing ductal metaplasia (ducts, ADM, PanIN and PDAC) or mucinous lesions (PanIN and some tumors) with CK19 or Alcian blue staining, respectively, similarly showed that female PK-*Insr*$^{w/w}$ mice formed significantly more lesions than female PK-*Insr*$^{f/f}$ mice (Extended Data 5A-C and 6A-C). Notably, male PK-*Insr*$^{w/w}$ mice likely had a similar amount of Alcian blue^{+} area compared to other genotypes due of the presence of higher-grade PanIN lesions that were Alcian blue negative. Additionally, there were more large cysts with predominantly normal epithelial present throughout the male PK-*Insr*$^{w/w}$ pancreata that were not frequently observed in females that could explain a lower than expected Alcian blue area, but result in high Ck19+ area in males (Figure 2A and Extended Data 5A, 5C, 6A, 6C). Consistent with PK-*Insr*$^{w/w}$ male progressing more quickly and thus, having less normal pancreas than PK-*Insr*$^{f/f}$ mice, quantification of acinar cell area showed that male PK-*Insr*$^{w/w}$ mice had little normal acinar area (0.1-5%) (Fig. 2F). Indeed, most male PK-*Insr*$^{w/w}$ and some female PK-*Insr*$^{w/w}$ pancreata were also comprised of almost all CK19^{+} area (maximum value for this metric is ~20-30% due to stroma

expansion) and little acinar area (Extended Data 6D-E). In contrast, as the representative pancreatic sections show, there were still large areas of normal acinar cells present in PK-*Insr*$^{f/f}$ mice compared to the other two genotypes (Fig. 2A-B and Extended Data 6D-E). In females, where fewer retention cysts were observed (Fig. 2B), likely due to the earlier stage of disease, more normal acinar area (2-45%) was retained in female PK-*Insr*$^{w/w}$ compared to male PK-*Insr*$^{w/w}$ mice. Importantly, significantly more acinar area was present in female PK-*Insr*$^{w/f}$ and PK-*Insr*$^{f/f}$ mice compared to PK-*Insr*$^{w/w}$ mice (Fig. 2F). Our data strongly suggested that acinar cell *Insr* dose-dependently regulates oncogenic Kras-induced PanINs in the context of diet-induced hyperinsulinemia.

Loss of *Insr* in *Kras*^{G12D}-expressing acinar cells reduced PanIN initiation

Data described above showed that PK-*Insr*$^{w/w}$ males, and some PK-*Insr*$^{w/f}$ males, may have reached their maximum capacity for ductal metaplasia after ~10 months on HFD. Therefore, we examined 12-week-old male and female mice of each genotype to test whether loss of Insr equally affects male and females' capacity for PanIN initiation. The pancreas weight to body weight ratios of *Ptf1a*^{CreER};*Insr*$^{w/w}$;nTnG and *Ptf1a*^{CreER};*Insr*$^{f/f}$;nTnG mice were not different (Extended Data. 7A), nor was there a significant difference between PK-*Insr*$^{w/w}$, PK-*Insr*$^{w/f}$, and PK-*Insr*$^{f/f}$ mice in either sex (Extended Data. 7B). This is consistent with previous data showing only a minority of the pancreas is affected in young *Ptf1a*^{CreER};*Kras*$^{LSL-G12D}$ mice[27]. At 12 weeks of age, acinar cells and PanIN lesions were also GFP positive indicating a good recombination efficiency (Extended Data 8A-B). Moreover, pancreata were predominantly normal with some ductal lesions having characteristics of ADM or low-grade PanIN (Fig. 3A-B). In males, there was a ~5.3-fold reduction in PanIN between PK-*Insr*$^{f/f}$ and PK-*Insr*$^{w/w}$ mice (Fig. 3C). In females, there was a ~6.3-fold reduction in PanIN between PK-*Insr*$^{f/f}$ and PK-*Insr*$^{w/w}$ mice and a significant ~3.5-fold reduction between PK-*Insr*$^{w/w}$ and PK-*Insr*$^{w/f}$ mice (Fig. 3C). Consistent with the PanIN analyses, there was more Sirius red-positive desmoplastic reaction in PK-*Insr*$^{w/w}$ mice compared to PK-*Insr*$^{f/f}$ mice (Extended Data 8C-E). These data indicate that Insr also contributes to early PanIN initiation in both sexes.

Proteomic and phospho-proteomic analyses of pancreata from mice lacking acinar *Insr*

To investigate the underlying molecular mechanisms of reduced PanIN initiation, we conducted unbiased proteomic analysis using the head of the pancreas from the 12-week-old female mice (Fig. 3) with and without Kras^{G12D} and/or *Insr*. We obtained reliable, quantitative data on 2889 proteins across all the samples. We focused first on the comparison between *Ptf1a*^{CreER};*Insr*$^{w/w}$;nTnG and PK-*Insr*$^{w/w}$ pancreata, we found that 124 proteins were upregulated and 122 were down-regulated as a consequence of expressing *Kras*^{G12D} (Extended Data 9A). Mutant *Kras*^{G12D} increased proteins associated with inflammation and PanIN including Reg3a, Reg3b, Reg2, Gkn1, and Gkn2[38-40] (Extended Data Fig 9A). This list could also be used to identify new markers of early-stage pancreatic

tumorigenesis. We also found 92 proteins increased expression and 155 proteins decreased expression because of losing Insr in Kras wild-type mice (Extended Data 9B).

To define the molecular mechanisms associated with *Insr* deletion in the context of mutant Kras, we focused further analyses on comparing to PK-*Insr*$^{f/f}$ pancreata to the PK-*Insr*$^{w/w}$ pancreata. We found 135 proteins that were upregulated in PanIN-reduced PK-*Insr*$^{f/f}$ mice compared to PK-*Insr*$^{w/w}$ controls, including the first enzyme of the fatty acid beta-oxidation pathway (Acox1), components of complex I of the mitochondrial electron transport chain (Ndufa11, Ndufa4), and Lemd3, a repressor of TGF-beta, Activin, and BMP signaling (Fig. 4A). Protection from PanIN formation in PK-*Insr*$^{f/f}$ pancreata was associated with 117 down-regulated proteins, including components of the electron transport chain at complex III (Uqcc2) and complex IV of (Cox6c, Cox7a), gastrokinins (Gkn1, Gkn2), markers of pancreatic inflammation (Reg3b, Reg3g), and exosome component 9 (Exosc9) (Fig. 4A). As a parallel analysis strategy, we performed a K-means clustering analysis with the differentially abundant genes between PK-*Insr*$^{w/w}$ and PK-*Insr*$^{f/f}$ mice) using the protein abundance values in all genotypes to identify patterns that varied by Insr status, Kras mutation, or both (Extended Data 9C). This revealed the coordinated down-regulation of digestive enzymes, including amylases (Amy1, Amy2), lipases (Pnliprp2, Pnliprp1, Pnlip, Cel), elastases (Cela1, Cela2a, Cela3b), carboxypeptidases (Cpa1, Cpa2), chymotrypsin (Ctrb1), and trypsin (Prss2) in PK-*Insr*$^{f/f}$ mice (Fig. 4B). Conversely, chymotrypsin C (Ctrc) and a secreted phospholipase A2 (Pla2g1b) were increased (Fig. 4B). This suggested a specific loss of some, but not all secreted pancreatic enzymes; and arguing against a general loss of protein synthesis or zymogen granule biogenesis or a general cell composition bias against acinar cells in the pancreas.

In order to investigate potential functional enrichment based on cell signaling, intracellular localization, and biological process, we further filtered for the most differentially abundant proteins between PK-*Insr*$^{w/w}$ and PK-*Insr*$^{f/f}$ mice (Adj. $p<0.05$ and $abs(log_2(Fold\ Change)) > 2.5$) and performed protein-protein interaction network cluster analysis using STRING[31] and assigned these proteins to their intracellular organelle locations or functions using COMPARTMENTS[41] (Fig. 4C). This analysis highlighted upregulation of proteins with key roles in mRNA splicing, protein synthesis at the ribosome, protein processing at the ER and Golgi, endosomes/lysosomes, and the cytoskeleton (Fig. 4C). Individual increased proteins with strong, direct network links to Insr or key insulin signaling components (e.g., Kras, Akt, mTor, Mapk1) included Creb1, Sh3gl1, Ptpn1, Gna14, Rbm8a, and Pla2g1b. Insulin-like growth factor 2 receptor protein levels were decreased. Together, these proteomic data identify protein networks that mediate protection from PDAC initiation from acinar cells with reduced Insr.

Parallel phosphoproteomic analysis on the same samples confirmed and extended the findings from our total proteomic analysis. We identified 225 downregulated phospho-peptides and 177 upregulated phospho-peptides comparing PK-*Insr*$^{f/f}$ pancreas to PK-*Insr*$^{w/w}$ controls (Fig. 5A). In

general, statistically significant phospho-peptides differences were not due to underlying differences in total protein abundance (Fig. 5B). Robust and significant decreases in phosphorylation were found on regulators of protein translation elongation (Eef1b, Eef1d) and initiation (Eif5b), as well as on Cavin3, which has been implicated in Akt-Erk signaling bias[42] (Fig.5B). Increased phosphorylation was found on components of the spliceosome (Srrm1, Srrm2), a cytoskeletal regulator (Dock7), a key lipid droplet associated protein (Plin1), and an antiapoptotic factor (Bclaf1) (Fig. 5B). Interestingly, multiple sites on the cholecystokinin (CCK) receptor (Cckar) showed altered phosphorylation (Fig. 5A-C), including sites in the main intracellular loop that are indicative of ligand-induced desensitization[43] and phospho-sites in the C-terminal tail that have not been previously reported. We also conducted a complementary statistical analysis that normalized phospho-peptides to their corresponding total protein determination (see Methods). This narrowed our focus to a subset of proteins that were largely increased by Kras and reversed with *Insr* knockout (Fig. 5D). PhosphoSite analysis revealed that a majority of these proteins have been previously identified as insulin responsive (Fig. 5E). Several of the differentially-phosphorylated residues are known targets of Pi3k/Akt or Kras signaling (Fig. 5E). Interestingly, we identified a differentially phosphorylated peptide from the pro-glucagon precursor, within the sequence of glucagon-like peptide 2, but the significance of this remains to be tested (Fig. 5E). Collectively, these unbiased total and phospho-proteomic studies delineate the possible molecular mechanisms by which hyperinsulinemia, acting via the Insr, may promote Kras-driven pancreatic cancer initiation.

Discussion

The purpose of this study was to test the hypothesis that hyperinsulinemia in the obese state acts directly on acinar cells to promote pancreatic cancer initiation. Our data clearly support a model where insulin receptor plays a causal role in supporting cancer initiation in the context of diet-induced obesity and mutant Kras. The contribution of direct insulin action on acinar cells is substantial, but does not preclude roles for Insr in other local or distant cell types[8]. Our unbiased proteomic and phospho-proteomic analyses enabled us to delineate multiple molecular mechanisms by which the insulin receptor affects the propensity of acinar cells to form PanIN formation and PDAC initiation in the context of obesity.

Diet-induced obesity induces basal insulin hypersecretion, increases β cell mass and impairs insulin clearance, resulting in sustained hyperinsulinemia[4,9]. As expected, mice used in this study, which had the full complement of all 4 insulin alleles (*Ins1* and *Ins2*), exhibited higher fasting insulin levels (males 1000-1500 pmol/L; females 500 pmol/L) than our previous models with insulin gene dosage reduced to 1 or 2 copies (males, 400-800 pmol/L; females 100-200 pmol/L[7,8]). Consistent with the hypothesis that endogenous hyperinsulinemia contributes to pancreatic cancer development, more than 90% of the normal pancreatic area in the PK-*Insr*$^{w/w}$ mice in this study was replaced by ductal

metaplasia, PanIN, and tumors at 10 months of age. Notably, 1-year-old PK-*Ins1*$^{+/+}$;*Ins2*$^{-/-}$ control mice had ~25% of the pancreas replaced by PanINs, while PK-*Ins1*$^{-/-}$;*Ins2*$^{+/+}$ mice were at just ~1-4% by 1 year of age[7,8]. If only considering PDAC, ~70% of female PK-*Insr*$^{w/w}$ mice developed PDAC in this study at 10 months of age, while only 1 female PK-*Ins1*$^{+/+}$;*Ins2*$^{-/-}$ mouse developed PDAC after a year[7,8]. Together, these findings suggest that simply reducing insulin production limits PanIN initiation in the context of obesity.

All cells in the body have insulin receptors and require insulin signaling for key functions, including nutrient uptake for storage and anabolism. While the roles of Insr in hepatocytes, myocytes, and adipocytes are well studied[44-46], the consequences of *Insr* loss in pancreatic acinar cells remain understudied. In this study, we specifically deleted the *Insr* gene from acinar cells using the *Ptf1a*^{CreER} allele and showed that insulin insensitivity in acinar cells had no obvious effects on systemic glucose homeostasis or serum insulin levels regardless of the *Kras* gene status. This suggests that the systemic regulation of glucose and insulin homeostasis are as expected in our mice fed HFD. Our data, combined with our previous studies[7,8], effectively rule out an essential role for hyperglycemia in PanIN and PDAC formation, but do not preclude potentially important roles for hyperglycemia in the later stages of disease[47,48].

Insulin receptor signaling activates PI3K/AKT/mTOR and MAPK/ERK signaling cascades, both of which have mitogenic effects. Effector proteins in these two pathways are frequently mutated during tumorigenesis[49-51], including in pancreatic cancer. Indeed, activating mutations in Kras, a key mediator of insulin and insulin-like growth factor signaling, drive the vast majority of pancreatic cancers[13]. Previous *in vitro* evidence supported the concept that hyperinsulinemia could promote cancer cell growth through over-activating the signaling cascades downstream of Insr protein[3,52,53]. Our findings are the first *in vivo* studies in any cancer type to demonstrate a direct causal role for hyperinsulinemia in the cancer cell of origin.

Mechanistically, our proteomic data demonstrated that *Insr* loss in acinar cells results in the coordinated reduction in digestive enzymes, with or without mutant Kras. This indicates that insulin signaling normally supports exocrine function. This is consistent with previous studies, including the observation that amylase production is diminished by β-cell ablation using streptozotocin and restored with insulin injection[54-56]. Mutations that result in increased trypsin activity in the pancreas[35], as well as animal studies using the CCK analog, caerulein, to stimulate enzyme secretion at supraphysiological levels[57], have demonstrated that tight control of digestive enzyme function reduces the risk of forming PDAC. Interestingly, our phospho-proteomic data identified hyper-phosphorylation of the CCKA receptor in Insr-knockout pancreas, linking local insulin signaling to CCK, a key endogenous regulator of acinar cell function and pancreatic weight. CCK secretion from I-cells is stimulated by the presence of amino acids and fat, which induces the highest I-cell secretion responses, in the small intestine[58]. CCK affects pancreatic secretions predominately through local action on nerve fibres in the gut to

induce a vago-vagal reflex circuit resulting in acetylcholine secretion from nerves in the pancreas. Alternatively, it also can act directly on murine acinar cells through the CCKA receptor. In addition to mediating digestive enzyme release from acinar cells, previous studies have also shown that injecting low levels of CCK into mice results in increased pancreatic size over time[59,60]. This suggests that CCK helps regulate the enzyme production capacity of the pancreas. Finally, it has been reported that HFD-associated inflammation can also promote islet CCK expression, which was proposed to play a role in obesity-associated PanIN formation[61]. However, our data suggested that the action of Insr signaling on PanIN formation may be upstream of the increased inflammation associated with HFD and regulate digestive enzyme production. This supports a working model whereby hyperinsulinemia promotes PanIN initiation via increased local inflammation associated with elevated digestive enzyme production and/or release. *Insr* loss in acinar cells may counter the increased signal for acinar cell enzyme production or cell proliferation induced by HFD. Further studies are needed to fully understand the impact of dietary content on acinar cells and their susceptibility to $Kras^{G12D}$-mediated transformation.

Our proteomic analyses also revealed other key mechanisms associated with suppressed pancreatic cancer initiation from acinar cells lacking *Insr*. For example, mRNA splicing and translation factors, known targets of insulin signaling[45], are differentially abundant in the pancreas after *Insr* loss in $Kras^{G12D}$-expressing acinar cells, suggesting possible mechanisms by which insulin might regulate the production of digestive enzymes. We also found evidence that reduced insulin signaling affected cellular metabolism. Previous studies have suggested that insulin can promote glycolysis in wildtype acinar cells to protect them during pancreatitis[62], however, detailed analyses of cell-type-specific mechanisms await single-cell cell proteomic and single-cell metabolomic characterization of this model.

We acknowledge the limitations of our study. One limitation of our study, and the field, is that existing antibody reagents are not specific enough to perform accurate anti-Insr staining that would allow us to determine whether acinar cells with normal morphology had escaped recombination at the *Insr* floxed allele. Another limitation is that, while our proteomic analysis provided quantification of 2889 protein abundances and 8787 phospho-sites, coverage of the proteome is not complete and biased against membrane proteins. For example, analysis of the abundance and phosphorylation of Igf1r, a protein that could compensate in *Insr* knockout cells, will require targeted assays and/or membrane fractionation. Insulin can bind to homodimeric Igf1 receptors and heterodimeric Insr/Igf1r hybrids, although at a lower affinity[19,63], to mediate its pro-tumourigenic effects. Nevertheless, it is clear that simply reducing *Insr* gene dosage was sufficient to reduce the effects of hyperinsulinemia on PanIN initiation. While we were unable to assess the role of Igf1r, future studies examining acinar cell-specific *Igf1r* loss in the presence or absence of concomitant *Insr* loss would be necessary to delineate any contribution to PanIN formation.

In summary, our data strongly suggest that insulin receptor signaling in acinar cells contributes to the PanIN and PDAC development. Our data illustrate the complex and interconnected molecular mechanisms by which hyperinsulinemia, acting directly through acinar cell Insr, promotes pancreatic tumourigenesis. We can infer that targeting insulin receptor signaling pathways, or hyperinsulinemia itself, may be beneficial in treating and preventing pancreatic cancer.

References

1 Rahib, L. *et al.* Projecting cancer incidence and deaths to 2030: the unexpected burden of thyroid, liver, and pancreas cancers in the United States. *Cancer Res* **74**, 2913-2921, doi:10.1158/0008-5472.CAN-14-0155 (2014).

2 Ilic, M. & Ilic, I. Epidemiology of pancreatic cancer. *World J Gastroenterol* **22**, 9694-9705, doi:10.3748/wjg.v22.i44.9694 (2016).

3 Gallagher, E. J. & LeRoith, D. Hyperinsulinaemia in cancer. *Nat Rev Cancer* **20**, 629-644, doi:10.1038/s41568-020-0295-5 (2020).

4 Zhang, A. M. Y., Wellberg, E. A., Kopp, J. L. & Johnson, J. D. Hyperinsulinemia in Obesity, Inflammation, and Cancer. *Diabetes Metab J* **45**, 622, doi:10.4093/dmj.2021.0131 (2021).

5 Stolzenberg-Solomon, R. Z. *et al.* Insulin, glucose, insulin resistance, and pancreatic cancer in male smokers. *JAMA* **294**, 2872-2878, doi:10.1001/jama.294.22.2872 (2005).

6 Pisani, P. Hyper-insulinaemia and cancer, meta-analyses of epidemiological studies. *Arch Physiol Biochem* **114**, 63-70, doi:10.1080/13813450801954451 (2008).

7 Zhang, A. M. Y. *et al.* Endogenous Hyperinsulinemia Contributes to Pancreatic Cancer Development. *Cell Metab* **30**, 403-404, doi:10.1016/j.cmet.2019.07.003 (2019).

8 Zhang, A. M. Y. *et al.* Effects of hyperinsulinemia on pancreatic cancer development and the immune microenvironment revealed through single-cell transcriptomics. *Cancer Metab* **10**, 5, doi:10.1186/s40170-022-00282-z (2022).

9 Mehran, A. E. *et al.* Hyperinsulinemia drives diet-induced obesity independently of brain insulin production. *Cell Metab* **16**, 723-737, doi:10.1016/j.cmet.2012.10.019 (2012).

10 Templeman, N. M. *et al.* Reduced Circulating Insulin Enhances Insulin Sensitivity in Old Mice and Extends Lifespan. *Cell Rep* **20**, 451-463, doi:10.1016/j.celrep.2017.06.048 (2017).

11 Templeman, N. M., Clee, S. M. & Johnson, J. D. Suppression of hyperinsulinaemia in growing female mice provides long-term protection against obesity. *Diabetologia* **58**, 2392-2402, doi:10.1007/s00125-015-3676-7 (2015).

12 Chan, D. S. *et al.* Body mass index and survival in women with breast cancer-systematic literature review and meta-analysis of 82 follow-up studies. *Ann Oncol* **25**, 1901-1914, doi:10.1093/annonc/mdu042 (2014).

13 Waters, A. M. & Der, C. J. KRAS: The Critical Driver and Therapeutic Target for Pancreatic Cancer. *Cold Spring Harb Perspect Med* **8**, doi:10.1101/cshperspect.a031435 (2018).

14 Heestand, G. M. & Kurzrock, R. Molecular landscape of pancreatic cancer: implications for current clinical trials. *Oncotarget* **6**, 4553-4561, doi:10.18632/oncotarget.2972 (2015).

15 Janku, F. *et al.* PIK3CA mutation H1047R is associated with response to PI3K/AKT/mTOR signaling pathway inhibitors in early-phase clinical trials. *Cancer Res* **73**, 276-284, doi:10.1158/0008-5472.CAN-12-1726 (2013).

16 Payne, S. N. *et al.* PIK3CA mutations can initiate pancreatic tumorigenesis and are targetable with PI3K inhibitors. *Oncogenesis* **4**, e169, doi:10.1038/oncsis.2015.28 (2015).

17 Sivaram, N. *et al.* Tumor-intrinsic PIK3CA represses tumor immunogenecity in a model of pancreatic cancer. *J Clin Invest* **129**, 3264-3276, doi:10.1172/JCI123540 (2019).

18 Hopkins, B. D. *et al.* Suppression of insulin feedback enhances the efficacy of PI3K inhibitors. *Nature* **560**, 499-503, doi:10.1038/s41586-018-0343-4 (2018).

19 Belfiore, A. *et al.* Insulin Receptor Isoforms in Physiology and Disease: An Updated View. *Endocr Rev* **38**, 379-431, doi:10.1210/er.2017-00073 (2017).

20 Aljada, A. *et al.* Quantification of insulin receptor mRNA splice variants as a diagnostic tumor marker in breast cancer. *Cancer Biomark* **15**, 653-661, doi:10.3233/CBM-150505 (2015).
21 Law, J. H. *et al.* Phosphorylated insulin-like growth factor-i/insulin receptor is present in all breast cancer subtypes and is related to poor survival. *Cancer Res* **68**, 10238-10246, doi:10.1158/0008-5472.CAN-08-2755 (2008).
22 Pan, F. C. *et al.* Spatiotemporal patterns of multipotentiality in Ptf1a-expressing cells during pancreas organogenesis and injury-induced facultative restoration. *Development* **140**, 751-764, doi:10.1242/dev.090159 (2013).
23 Tuveson, D. A. *et al.* Endogenous oncogenic K-ras(G12D) stimulates proliferation and widespread neoplastic and developmental defects. *Cancer Cell* **5**, 375-387, doi:10.1016/s1535-6108(04)00085-6 (2004).
24 Prigge, J. R. *et al.* Nuclear double-fluorescent reporter for in vivo and ex vivo analyses of biological transitions in mouse nuclei. *Mamm Genome*, doi:10.1007/s00335-013-9469-8 (2013).
25 Bruning, J. C. *et al.* A muscle-specific insulin receptor knockout exhibits features of the metabolic syndrome of NIDDM without altering glucose tolerance. *Mol Cell* **2**, 559-569, doi:10.1016/s1097-2765(00)80155-0 (1998).
26 Søs Skovsø, E. P., Jelena Kolic, Haoning Howard Cen, Derek A. Dionne, Xiao-Qing Dai, Rohit B. Sharma, Lynda Elghazi, Cara E. Ellis, Katharine Faulkner, Stephanie A.M. Marcil, Peter Overby, Nilou Noursadeghi, Daria Hutchinson, Xiaoke Hu, Hong Li, Honey Modi, Jennifer S. Wildi, J. Diego Botezelli, Hye Lim Noh, Sujin Suk, Brian Gablaski, Austin Bautista, Ryekjang Kim, Cras-Méneur, Stephane Flibotte, Sunita Sinha, Dan S. Luciani, Corey Nislow, Elizabeth J. Rideout, Eric N. Cytrynbaum, Jason K. Kim, Ernesto Bernal-Mizrachi, Laura C. Alonso, Patrick E. MacDonald, James D. Johnson. Beta-cell specific Insr deletion promotes insulin hypersecretion and improves glucose tolerance prior to global insulin resistance. *biRxiv* (2021).
27 Kopp, J. L. *et al.* Identification of Sox9-dependent acinar-to-ductal reprogramming as the principal mechanism for initiation of pancreatic ductal adenocarcinoma. *Cancer Cell* **22**, 737-750, doi:10.1016/j.ccr.2012.10.025 (2012).
28 Lee, A. Y. L. *et al.* Cell of origin affects tumour development and phenotype in pancreatic ductal adenocarcinoma. *Gut*, doi:10.1136/gutjnl-2017-314426 (2018).
29 HaileMariam, M. *et al.* S-Trap, an Ultrafast Sample-Preparation Approach for Shotgun Proteomics. *J Proteome Res* **17**, 2917-2924, doi:10.1021/acs.jproteome.8b00505 (2018).
30 Gu, Z., Eils, R. & Schlesner, M. Complex heatmaps reveal patterns and correlations in multidimensional genomic data. *Bioinformatics* **32**, 2847-2849, doi:10.1093/bioinformatics/btw313 (2016).
31 Szklarczyk, D. *et al.* The STRING database in 2021: customizable protein-protein networks, and functional characterization of user-uploaded gene/measurement sets. *Nucleic Acids Res* **49**, D605-D612, doi:10.1093/nar/gkaa1074 (2021).
32 Shannon, P. *et al.* Cytoscape: a software environment for integrated models of biomolecular interaction networks. *Genome Res* **13**, 2498-2504, doi:10.1101/gr.1239303 (2003).
33 Ritchie, M. E. *et al.* limma powers differential expression analyses for RNA-sequencing and microarray studies. *Nucleic Acids Res* **43**, e47, doi:10.1093/nar/gkv007 (2015).
34 Dawson, D. W. *et al.* High-fat, high-calorie diet promotes early pancreatic neoplasia in the conditional KrasG12D mouse model. *Cancer Prev Res (Phila)* **6**, 1064-1073, doi:10.1158/1940-6207.CAPR-13-0065 (2013).
35 Chang, H. H. *et al.* Incidence of pancreatic cancer is dramatically increased by a high fat, high calorie diet in KrasG12D mice. *PLoS One* **12**, e0184455, doi:10.1371/journal.pone.0184455 (2017).
36 Muzumdar, M. D., Tasic, B., Miyamichi, K., Li, L. & Luo, L. A global double-fluorescent Cre reporter mouse. *Genesis* **45**, 593-605, doi:10.1002/dvg.20335 (2007).
37 Berglund, E. D. *et al.* Glucose metabolism in vivo in four commonly used inbred mouse strains. *Diabetes* **57**, 1790-1799, doi:10.2337/db07-1615 (2008).

38 Chen, Z., Downing, S. & Tzanakakis, E. S. Four Decades After the Discovery of Regenerating Islet-Derived (Reg) Proteins: Current Understanding and Challenges. *Front Cell Dev Biol* **7**, 235, doi:10.3389/fcell.2019.00235 (2019).
39 Li, Q. *et al.* Reg proteins promote acinar-to-ductal metaplasia and act as novel diagnostic and prognostic markers in pancreatic ductal adenocarcinoma. *Oncotarget* **7**, 77838-77853, doi:10.18632/oncotarget.12834 (2016).
40 Steiner, S. *et al.* De novo expression of gastrokines in pancreatic precursor lesions impede the development of pancreatic cancer. *Oncogene* **41**, 1507-1517, doi:10.1038/s41388-022-02182-4 (2022).
41 Binder, J. X. *et al.* COMPARTMENTS: unification and visualization of protein subcellular localization evidence. *Database (Oxford)* **2014**, bau012, doi:10.1093/database/bau012 (2014).
42 Hernandez, V. J. *et al.* Cavin-3 dictates the balance between ERK and Akt signaling. *Elife* **2**, e00905, doi:10.7554/eLife.00905 (2013).
43 Rao, R. V., Holicky, E. L., Kuntz, S. M. & Miller, L. J. CCK receptor phosphorylation exposes regulatory domains affecting phosphorylation and receptor trafficking. *Am J Physiol Cell Physiol* **279**, C1986-1992, doi:10.1152/ajpcell.2000.279.6.C1986 (2000).
44 Cherrington, A. D. The role of hepatic insulin receptors in the regulation of glucose production. *J Clin Invest* **115**, 1136-1139, doi:10.1172/JCI25152 (2005).
45 Haeusler, R. A., McGraw, T. E. & Accili, D. Biochemical and cellular properties of insulin receptor signalling. *Nat Rev Mol Cell Biol* **19**, 31-44, doi:10.1038/nrm.2017.89 (2018).
46 Cen, H. H. *et al.* Human and mouse muscle transcriptomic analyses identify insulin receptor mRNA downregulation in hyperinsulinemia-associated insulin resistance. *FASEB J* **36**, e22088, doi:10.1096/fj.202100497RR (2022).
47 Sato, K. *et al.* Hyperglycemia enhances pancreatic cancer progression accompanied by elevations in phosphorylated STAT3 and MYC levels. *PloS one* **15**, e0235573-e0235573, doi:10.1371/journal.pone.0235573 (2020).
48 Vaziri-Gohar, A. *et al.* Increased glucose availability sensitizes pancreatic cancer to chemotherapy. *bioRxiv*, 2022.2004.2029.490090, doi:10.1101/2022.04.29.490090 (2022).
49 Samuels, Y. *et al.* High frequency of mutations of the PIK3CA gene in human cancers. *Science* **304**, 554, doi:10.1126/science.1096502 (2004).
50 Yang, J. *et al.* Targeting PI3K in cancer: mechanisms and advances in clinical trials. *Mol Cancer* **18**, 26, doi:10.1186/s12943-019-0954-x (2019).
51 Guo, Y. J. *et al.* ERK/MAPK signalling pathway and tumorigenesis. *Exp Ther Med* **19**, 1997-2007, doi:10.3892/etm.2020.8454 (2020).
52 Godsland, I. F. Insulin resistance and hyperinsulinaemia in the development and progression of cancer. *Clin Sci (Lond)* **118**, 315-332, doi:10.1042/CS20090399 (2009).
53 Zhang, A. M. Y., Wellberg, E. A., Kopp, J. L. & Johnson, J. D. Hyperinsulinemia in Obesity, Inflammation, and Cancer. *Diabetes Metab J* **45**, 285-311, doi:10.4093/dmj.2020.0250 (2021).
54 Henderson, J. R., Daniel, P. M. & Fraser, P. A. The pancreas as a single organ: the influence of the endocrine upon the exocrine part of the gland. *Gut* **22**, 158-167, doi:10.1136/gut.22.2.158 (1981).
55 Soling, H. D. & Unger, K. O. The role of insulin in the regulation of -amylase synthesis in the rat pancreas. *Eur J Clin Invest* **2**, 199-212, doi:10.1111/j.1365-2362.1972.tb00645.x (1972).
56 Frier, B. M., Saunders, J. H., Wormsley, K. G. & Bouchier, I. A. Exocrine pancreatic function in juvenile-onset diabetes mellitus. *Gut* **17**, 685-691, doi:10.1136/gut.17.9.685 (1976).
57 Guerra, C. *et al.* Chronic pancreatitis is essential for induction of pancreatic ductal adenocarcinoma by K-Ras oncogenes in adult mice. *Cancer Cell* **11**, 291-302, doi:10.1016/j.ccr.2007.01.012 (2007).
58 Otsuki, M. Pathophysiological role of cholecystokinin in humans. *J Gastroenterol Hepatol* **15 Suppl**, D71-83, doi:10.1046/j.1440-1746.2000.02178.x (2000).
59 Varga, G. *et al.* Caerulein in supramaximal doses fails to stimulate pancreatic growth, but it forces secretory granulopoiesis. *Acta Physiol Hung* **71**, 99-106 (1988).

60 DEMBINSKI, A. B. & JOHNSON, L. R. Stimulation of Pancreatic Growth by Secretin, Caerulein, and Pentagastrin*. *Endocrinology* **106**, 323-328, doi:10.1210/endo-106-1-323 (1980).
61 Incio, J. *et al.* Obesity-Induced Inflammation and Desmoplasia Promote Pancreatic Cancer Progression and Resistance to Chemotherapy. *Cancer Discov* **6**, 852-869, doi:10.1158/2159-8290.CD-15-1177 (2016).
62 Bruce, J. I. E. *et al.* Insulin protects acinar cells during pancreatitis by preserving glycolytic ATP supply to calcium pumps. *Nat Commun* **12**, 4386, doi:10.1038/s41467-021-24506-w (2021).
63 Belfiore, A., Frasca, F., Pandini, G., Sciacca, L. & Vigneri, R. Insulin receptor isoforms and insulin receptor/insulin-like growth factor receptor hybrids in physiology and disease. *Endocr Rev* **30**, 586-623, doi:10.1210/er.2008-0047 (2009).

Figure Legends

Fig. 1. Loss of *Insr* in pancreatic acinar cells had no effect glucose homeostasis in *Ptf1a*^{CreER}-induced *Kras*^{G12D} pancreatic cancer model.

A, Schematic describing a mouse model designed to test the role of insulin receptor signaling on HFD-accelerated PDAC initiation. On the background of the *Ptf1a*^{CreER}-induced *Kras*^{G12D} pancreatic cancer model (PK), we generated mice having two wild-type *Insr* alleles (*Insr*$^{w/w}$), one *Insr* floxed allele (*Insr*$^{w/f}$), or two *Insr* floxed alleles (*Insr*$^{f/f}$). **B,** Three-week-old mice were weaned and provided high fat diet (HFD) for the duration of the study. At 4-weeks-old, they were injected with tamoxifen (TM) on 3 consecutive days. Physiological measures were taken every 3 months for 10 months, mice were euthanized at 12 or 43.5 weeks of age for histopathological analyses. **C-H,** Body weight (**C-D),** fasting blood glucose (**E-F)**, or fasting insulin (**G-H)** measurements for PK-*Insr*$^{w/w}$, PK-*Insr*$^{w/f}$, and PK-*Insr*$^{f/f}$ male (M:) (**C, E, G**) and female (F:) (**D, F, H**) mice (n= 13-33). Values shown as mean ± SEM.

Fig. 2. Loss of *Insr* in acinar cells reduced PanIN and PDAC formation.

A-B, Representative whole section (top) and high-magnification (bottom) H&E images of pancreatic slides from 43.5-week-old male (**A**) and female (**B**) PK-*Insr*$^{w/w}$, PK-*Insr*$^{w/f}$, and PK-*Insr*$^{f/f}$ mice. **C-F,** Quantification of PanIN plus tumor area (**C**)**,** PanIN only area (**D**), tumor area (**E**), or acinar cell area (F) in pancreata from each genotype and sex (M or F) (n= 5-16). Filled dots and triangles denoted mice that developed tumors in **C**. Scale bars: 2 mm (top) and 0.1mm (bottom). Values are shown as mean ± SEM. *p<0.05, **p<0.01, ***p<0.001, ****p<0.0001.

Fig. 3. Loss of *Insr* in acinar cells reduced PanIN lesions initiation.

A-B, Representative whole section (top) and high-magnification (bottom) H&E images of pancreatic slides from 12-week-old male (**A**) and female (**B**) PK-*Insr*$^{w/w}$, PK-*Insr*$^{w/f}$, and PK-*Insr*$^{f/f}$ mice. **C,** Quantification of PanIN area in pancreata from each genotype and sex (M or F) (n= 3-14). Scale bars: 2 mm (top) and 0.1mm (bottom). Values are shown as mean ± SEM. *p<0.05.

Fig. 4. Loss of *Insr* in acinar cells reduced digestive enzymes production in pancreas.

A, Volcano plot showing proteins that were significantly up- or down-regulated in PK-*Insr*$^{f/f}$ mice compared to PK-*Insr*$^{w/w}$ mice. **B**, Heatmap showing the change of protein abundance between genotypes for proteins involved in pancreatic digestive enzymes secretion. **C**, Differentially abundant proteins (Adj. p<0.05 and abs($\log_2$(Fold Change)) > 2.5) between PK-*Insr*$^{w/w}$ and PK-*Insr*$^{f/f}$ pancreata were connected using STRING and diagrammatically presented here in the context of Insr signaling and cellular organelles and functions. The color in each oval reflects the fold change, while the thickness of the line around the oval represents the Adj. p-value. Proteins depicted in white ovals were added to show the potential relationship of the differentially abundant proteins to insulin signaling.

Fig. 5. The phospho-proteomic analysis of insulin receptors' effects on PanIN initiation

A, Volcano plots for phospho-peptides that were significantly up or down regulated in PK-*Insr*$^{f/f}$ mice compared to PK-*Insr*$^{w/w}$ mice. **B**, Change in phospho-peptide abundance (Adj. p-values indicated in red) compared to the change in corresponding protein's abundance between PK-*Insr*$^{f/f}$ mice and PK-*Insr*$^{w/w}$ mice. **C**, TOP: Schematic of phosphorylation sites on Cckar that were differentially abundant in any comparison. BOTTOM: The relative phospho-peptide abundance (arbitrary units) for each detected phospho-peptide for all samples (white dots) and genotypes. **D**, A heatmap of the top 21 phospho-sites (normalized to their corresponding total protein level and sorted by Adj. p-value) that were differentially expressed between PK-*Insr*$^{w/w}$ and PK-*Insr*$^{f/f}$ mice. **E,** Intracellular locations of differentially phosphorylated proteins (in **D**) and their relationship to insulin and KRAS signaling. Proteins in yellow are known to be regulated by insulin. Pink arrows denote known insulin signaling mechanisms. Blue arrows indicate the proteins regulated at the identified phosphorylation sites in our dataset. Gray arrows indicate the proteins regulated in our dataset but not at the significantly different phosphorylation sites. Aspects of the Insr signaling cascade that were not differentially abundant (pink) are shown in the diagram for context. Values are shown as mean + SEM. *Adj. $p<0.05$, **Adj. $p<0.01$, ***Adj. $p<0.001$, ****Adj. $p<0.0001$.

Extended Data Fig. 1. Loss of *Insr* in pancreatic acinar cells had no effect on glucose homeostasis.

A, Schematic describing mouse models designed to test the role of insulin receptor signaling in pancreatic acinar cells. On the background of the *Ptf1a*^{CreER} mice, we generated mice having two wild-type *Insr* alleles (*Insr*$^{w/w}$) or two *Insr* floxed alleles (*Insr*$^{f/f}$). **B-G,** Body weight (**B-C**), fasting blood glucose (**D-E**), and fasting insulin (**F-G**) measurements in male (**B, D, F**) and female (**C, E, G**) *Ptf1a*^{CreER}-*Insr*$^{w/w}$ and *Ptf1a*^{CreER}-*Insr*$^{f/f}$ mice measured over >1 year (n= 10-17). Values are shown as mean ± SEM. *$p<0.05$.

Extended Data Fig. 2. The male mice without *Insr* had worst survival rate.

A, Percentage of mice of the indicated genotype that were found dead or reached humane endpoint throughout the study. The star symbol indicates whether a macroscopic mass was observed in the pancreas at necropsy, when possible. There were 8 PK-*Insr*$^{w/w}$, 20 PK-*Insr*$^{w/f}$, and 7 PK-*Insr*$^{f/f}$ male mice and 9 PK-*Insr*$^{w/w}$ 17 PK-*Insr*$^{w/f}$, and 12 PK-*Insr*$^{f/f}$ female mice in the cohort. At 43.5 weeks, the remaining mice were euthanized and assessed for presence of tumors.

Extended Data Fig. 3. The *Ptf1a*^{CreER} allele labeled acinar cells and PanINs.

A-B, Representative whole section (top) and high-magnification (bottom) images of immunohistochemical staining for GFP expressed from nTnG lineage tracing allele in 43.5-week-old male (**A**) and female (**B**) PK-*Insr*$^{w/w}$, PK-*Insr*$^{w/f}$, and PK-*Insr*$^{f/f}$ mice. Scale bars: 2 mm (top) and 0.1mm (bottom).

Extended Data Fig. 4. Histological effects were not detected in the absence of *Insr* in acinar cells.

A-B, Representative whole section (top) and high-magnification (bottom) images for immunohistochemical staining for GFP expressed from nTnG lineage tracing allele in 43.5-week-old male (A) and female (B) *Ptf1a*^{CreER}-*Insr*$^{w/w}$ and *Ptf1a*^{CreER}-*Insr*$^{f/f}$ mice. Scale bars: 2 mm (top) and 0.1mm (bottom).

Extended Data Fig. 5. Loss of Insr in acinar cells reduced Alcian blue+ PanIN lesions.

A-B, Representative whole section (top) and high-magnification (bottom) images of pancreatic slides from male (**A**) and female (**B**) PK-*Insr*$^{w/w}$, PK-*Insr*$^{w/f}$, and PK-*Insr*$^{f/f}$ mice stained with Alcian blue. **C,** Quantification of Alcian blue positive area for mice from each genotype and sex (M or F) (n= 5-16). Scale bars: 2 mm (top) and 0.1 mm (bottom). Values are shown as mean ± SEM. **p<0.01.

Extended Data Fig. 6. Loss of *Insr* in acinar cells reduced ductal metaplasia.

A-B, Representative whole section (top) and high-magnification (bottom) images of immunohistochemical staining of CK19 for male (**A**) and female (**B**) PK-*Insr*$^{w/w}$, PK-*Insr*$^{w/f}$, and PK-*Insr*$^{f/f}$ mice. **C,** Quantification of CK19^{+} area for mice from each genotype and sex (M or F) (n= 5-15). **D-E,** The correlation of acinar cell area and CK19^{+} area for male (**D**) and female (**E**) mice. Scale bars: 2 mm (top) and 0.1 mm (bottom). Values are shown as mean ± SEM. *p<0.05, **p<0.01, ***p<0.001, ****p<0.0001.

Extended Data Fig. 7. Loss of *Insr* in acinar cells had no effect on pancreas size.

A, The ratio of pancreatic weight to mouse body weight for male (M) and female (F) *Ptf1a*^{CreER}-*Insr*$^{w/w}$ and *Ptf1a*^{CreER}-*Insr*$^{f/f}$ mice (n= 3-6). **B,** The ratio of pancreatic weight to mouse body weight for male (M) and female (F) PK-*Insr*$^{w/w}$, PK-*Insr*$^{w/f}$, and PK-*Insr*$^{f/f}$ mice (n= 3-15). Values are shown as mean ± SEM.

Extended Data Fig. 8. Loss of *Insr* in acinar cells reduced desmoplasia.

A-B, Representative whole section (top) and high-magnification (bottom) images of immunohistochemical staining for GFP expressed from the nTnG lineage tracing allele in 12-week-old male (**A**) and female (**B**) PK-*Insr*$^{w/w}$, PK-*Insr*$^{w/f}$, and PK-*Insr*$^{f/f}$ pancreata. **C-D,** Representative whole section (top) and high-magnification (bottom) images of pancreatic slides from male (**C**) and female (**D**) mice PK-*Insr*$^{w/w}$, PK-*Insr*$^{w/f}$, and PK-*Insr*$^{f/f}$ stained with Sirius red. **E,** Quantification of Sirius red positive area for mice from each genotype and sex (M or F) (n= 3-4). Scale bars: GFP: 1mm (top) and 0.1 mm (bottom). Sirius Red: 2 mm (top) and 0.1 mm (bottom). Values are shown as mean ± SEM. *p<0.05.

Extended Data Fig. 9. The proteins differentially expressed due to either *Insr* deletion or *Kras*^{G12D}.

A, Volcano plot for proteins that were significantly up- or down-regulated in PK-*Insr*$^{w/w}$ mice compared to *Ptf1a*^{CreER}-*Insr*$^{w/w}$ mice. **B**, Volcano plot for proteins that were significantly up- or down-regulated in *Ptf1a*^{CreER}-*Insr*$^{f/f}$ mice compared to *Ptf1a*^{CreER}-*Insr*$^{w/w}$ mice. **C,** Proteins that were differentially abundant between PK-*Insr*$^{w/w}$ and PK-*Insr*$^{f/f}$ mice were selected and their abundance across all genotypes was used for k-means clustering. The clusters were visualized by heatmap to show their variance across all genotypes. The proteins in clusters 1, 2, 3, and 7 are listed in the order shown in the heatmap from top to bottom.

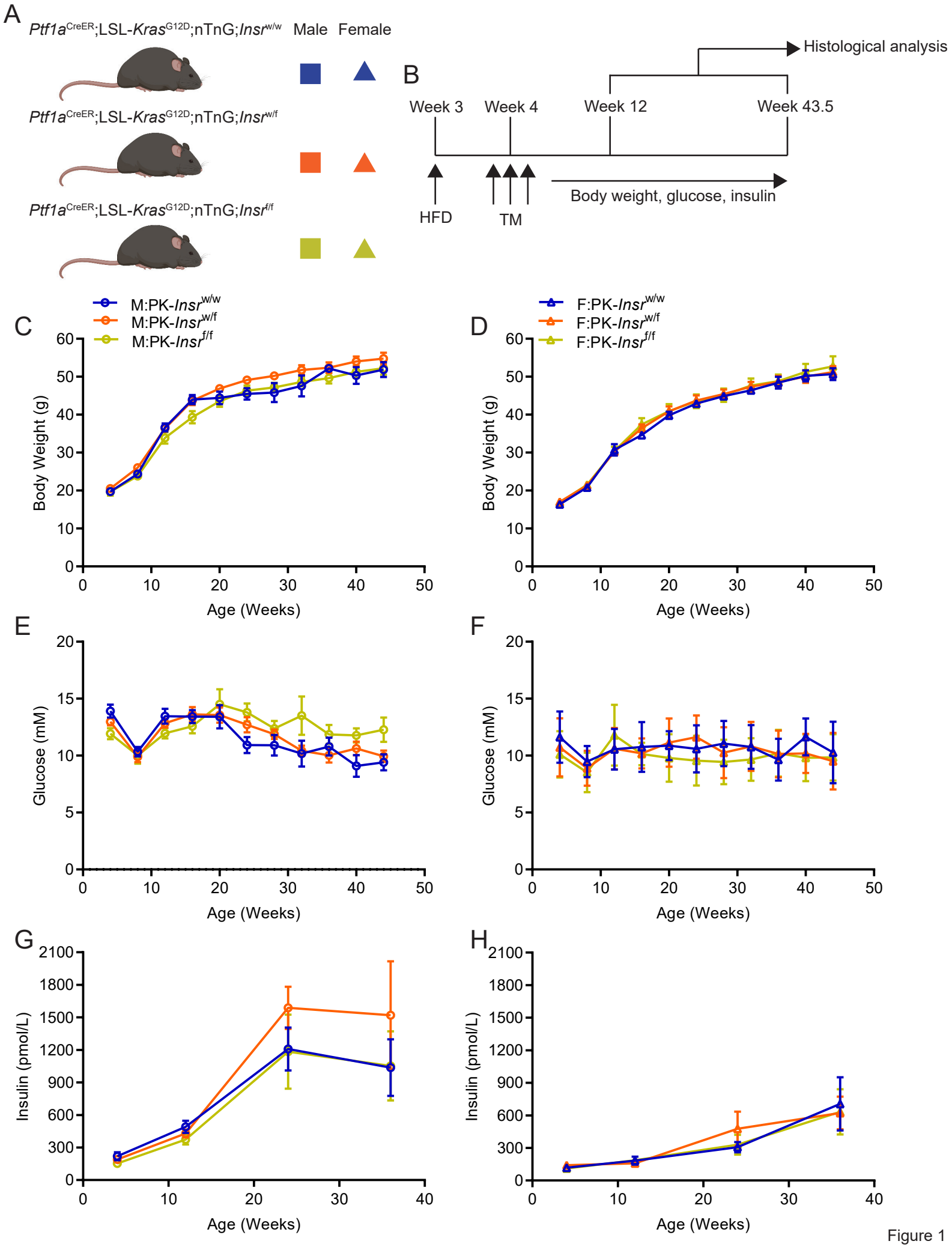
A
Ptf1aCreER;LSL-KrasG12D;nTnG;Insrw/w
Male
Female
Ptf1aCreER;LSL-KrasG12D;nTnG;Insrw/f
Ptf1aCreER;LSL-KrasG12D;nTnG;Insrf/f
B
Histological analysis
Week 3
Week 4
Week 12
Week 43.5
HFD
TM
Body weight, glucose, insulin
C
M:PK-Insrw/w
M:PK-Insrw/f
M:PK-Insrf/f
Body Weight (g)
Age (Weeks)
D
F:PK-Insrw/w
F:PK-Insrw/f
F:PK-Insrf/f
Body Weight (g)
Age (Weeks)
E
Glucose (mM)
Age (Weeks)
F
Glucose (mM)
Age (Weeks)
G
Insulin (pmol/L)
Age (Weeks)
H
Insulin (pmol/L)
Age (Weeks)

Figure 1

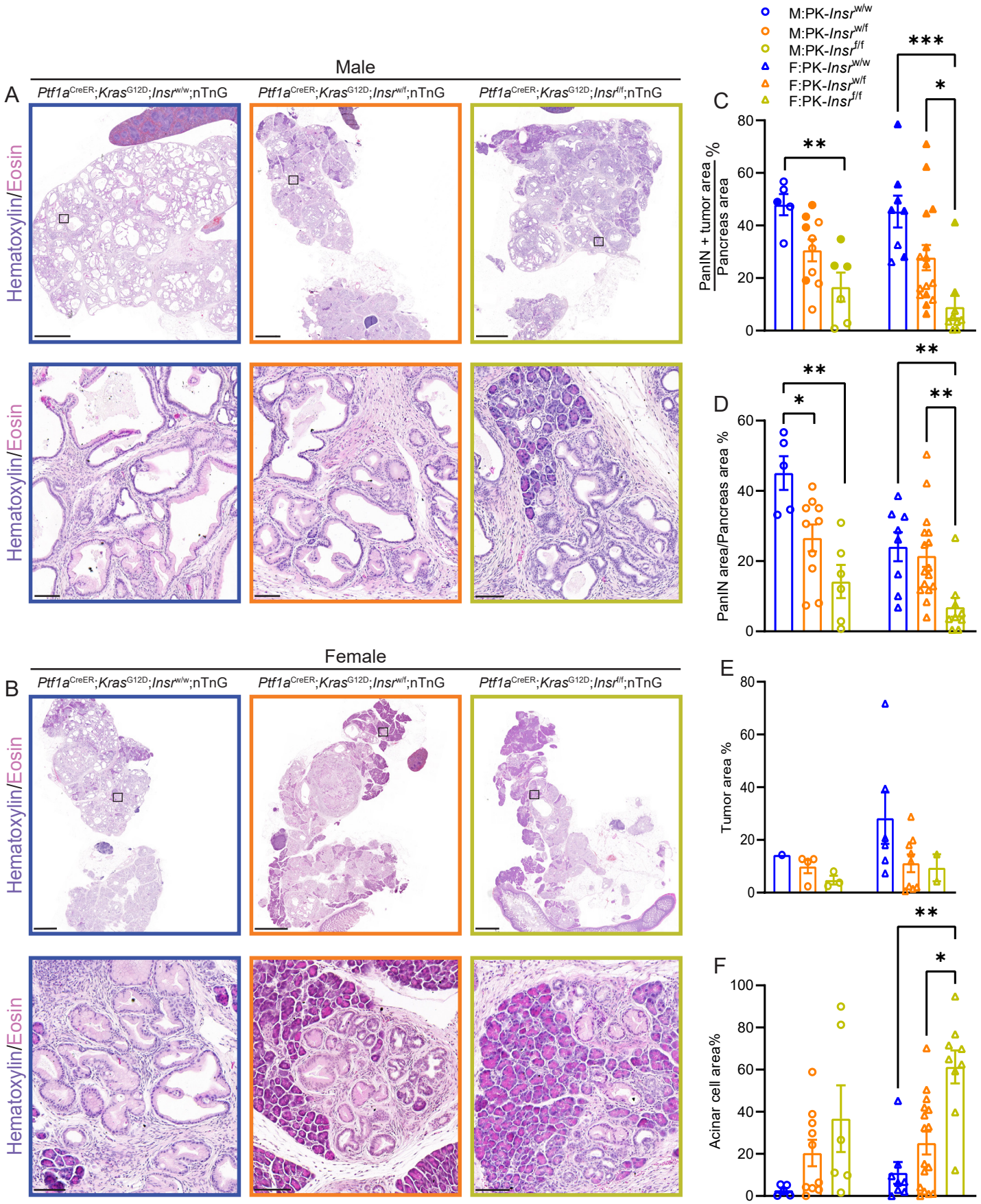
Male
A
Ptf1aCreER;KrasG12D;Insrw/w;nTnG
Ptf1aCreER;KrasG12D;Insrw/f;nTnG
Ptf1aCreER;KrasG12D;Insrf/f;nTnG
Hematoxylin/Eosin
Hematoxylin/Eosin
Female
B
Ptf1aCreER;KrasG12D;Insrw/w;nTnG
Ptf1aCreER;KrasG12D;Insrw/f;nTnG
Ptf1aCreER;KrasG12D;Insrf/f;nTnG
Hematoxylin/Eosin
Hematoxylin/Eosin
M:PK-Insrw/w
M:PK-Insrw/f
M:PK-Insrf/f
F:PK-Insrw/w
F:PK-Insrw/f
F:PK-Insrf/f
C
PanIN + tumor area / Pancreas area %
D
PanIN area/Pancreas area %
E
Tumor area %
F
Acinar cell area%

Figure 2

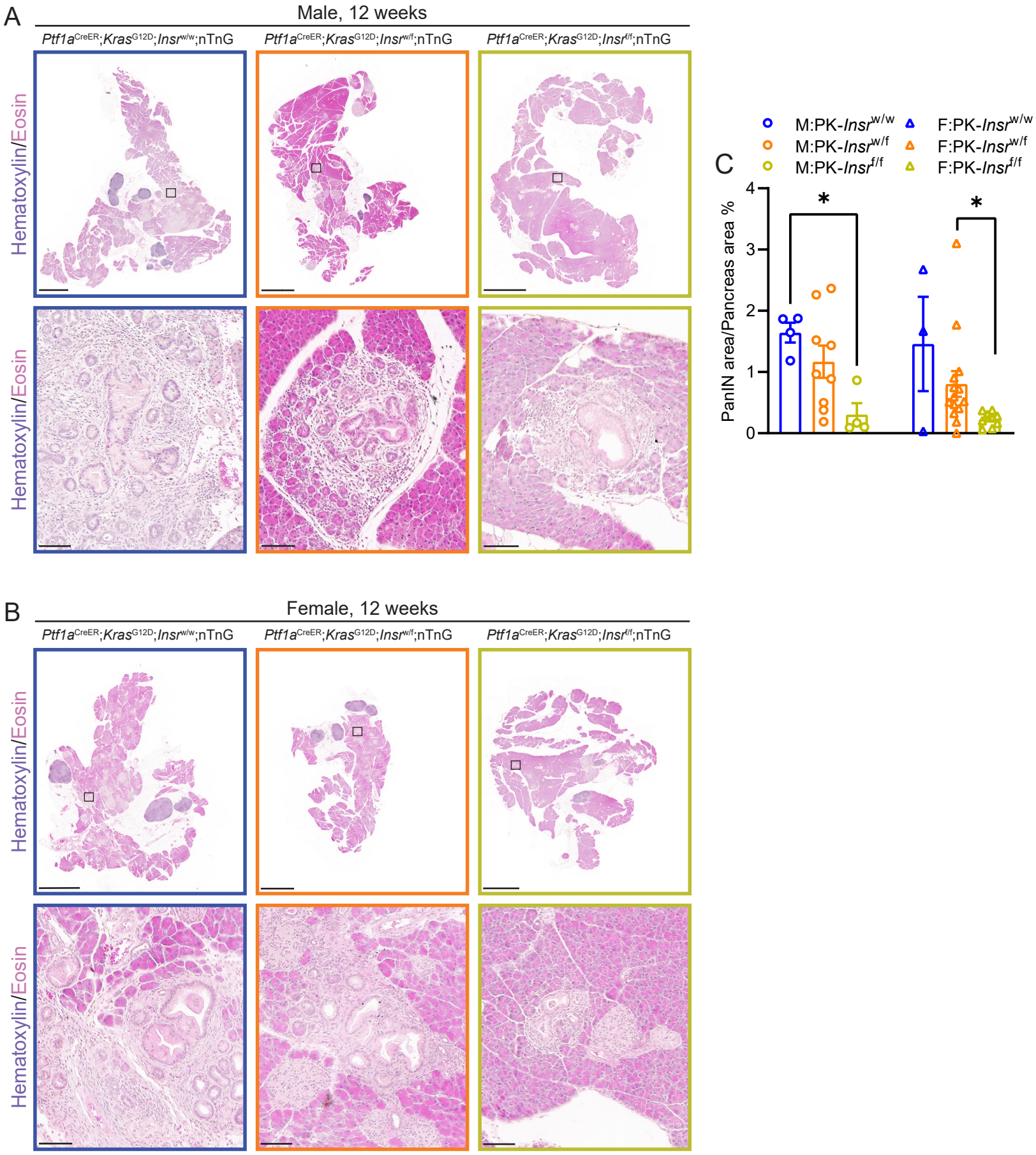
A
Male, 12 weeks
Ptf1aCreER;KrasG12D;Insrw/w;nTnG
Ptf1aCreER;KrasG12D;Insrw/f;nTnG
Ptf1aCreER;KrasG12D;Insrf/f;nTnG
Hematoxylin/Eosin
Hematoxylin/Eosin
B
Female, 12 weeks
Ptf1aCreER;KrasG12D;Insrw/w;nTnG
Ptf1aCreER;KrasG12D;Insrw/f;nTnG
Ptf1aCreER;KrasG12D;Insrf/f;nTnG
Hematoxylin/Eosin
Hematoxylin/Eosin
C
M:PK-Insrw/w
M:PK-Insrw/f
M:PK-Insrf/f
F:PK-Insrw/w
F:PK-Insrw/f
F:PK-Insrf/f
PanIN area/Pancreas area %
0
1
2
3
4
*
*

Figure 3

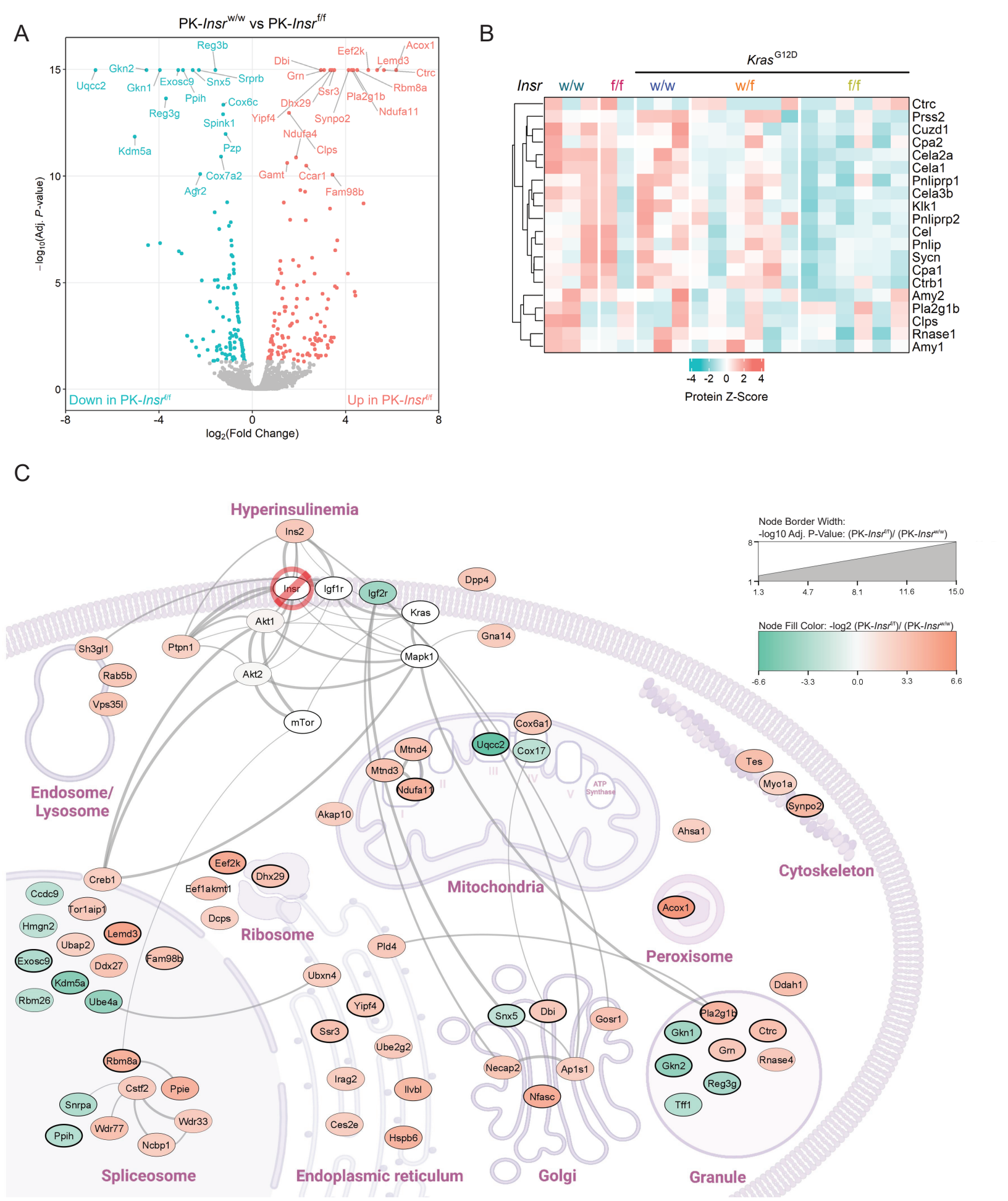
A
PK-Insr w/w vs PK-Insr f/f
Reg3b
Gkn2
Uqcc2
Gkn1
Exosc9
Snx5
Srprb
Ppih
Cox6c
Reg3g
Spink1
Kdm5a
Pzp
Cox7a2
Agr2
Dbi
Grn
Eef2k
Lemd3
Acox1
Ctrc
Rbm8a
Ssr3
Pla2g1b
Dhx29
Ndufa11
Yipf4
Synpo2
Ndufa4
Clps
Gamt
Ccar1
Fam98b
−log10(Adj. P-value)
log2(Fold Change)
Down in PK-Insr f/f
Up in PK-Insr f/f
B
Kras G12D
Insr
w/w
f/f
w/w
w/f
f/f
Ctrc
Prss2
Cuzd1
Cpa2
Cela2a
Cela1
Pnliprp1
Cela3b
Klk1
Pnliprp2
Cel
Pnlip
Sycn
Cpa1
Ctrb1
Amy2
Pla2g1b
Clps
Rnase1
Amy1
Protein Z-Score
C
Hyperinsulinemia
Ins2
Insr
Igf1r
Igf2r
Kras
Dpp4
Gna14
Akt1
Ptpn1
Mapk1
Akt2
mTor
Sh3gl1
Rab5b
Vps35l
Endosome/ Lysosome
Node Border Width:
-log10 Adj. P-Value: (PK-Insr f/f)/ (PK-Insr w/w)
Node Fill Color: -log2 (PK-Insr f/f)/ (PK-Insr w/w)
Cox6a1
Uqcc2
Cox17
Mtnd4
Mtnd3
Ndufa11
Akap10
ATP Synthase
Mitochondria
Tes
Myo1a
Synpo2
Ahsa1
Cytoskeleton
Creb1
Eef2k
Dhx29
Eef1akmt1
Dcps
Ccdc9
Tor1aip1
Hmgn2
Lemd3
Ubap2
Exosc9
Ddx27
Fam98b
Kdm5a
Rbm26
Ube4a
Ribosome
Pld4
Acox1
Peroxisome
Ubxn4
Yipf4
Ddah1
Snx5
Dbi
Gosr1
Ssr3
Ube2g2
Pla2g1b
Gkn1
Ctrc
Grn
Rnase4
Gkn2
Reg3g
Tff1
Rbm8a
Cstf2
Ppie
Snrpa
Wdr77
Wdr33
Ppih
Ncbp1
Spliceosome
Irag2
Ilvbl
Ces2e
Hspb6
Endoplasmic reticulum
Necap2
Ap1s1
Nfasc
Golgi
Granule

Figure 4

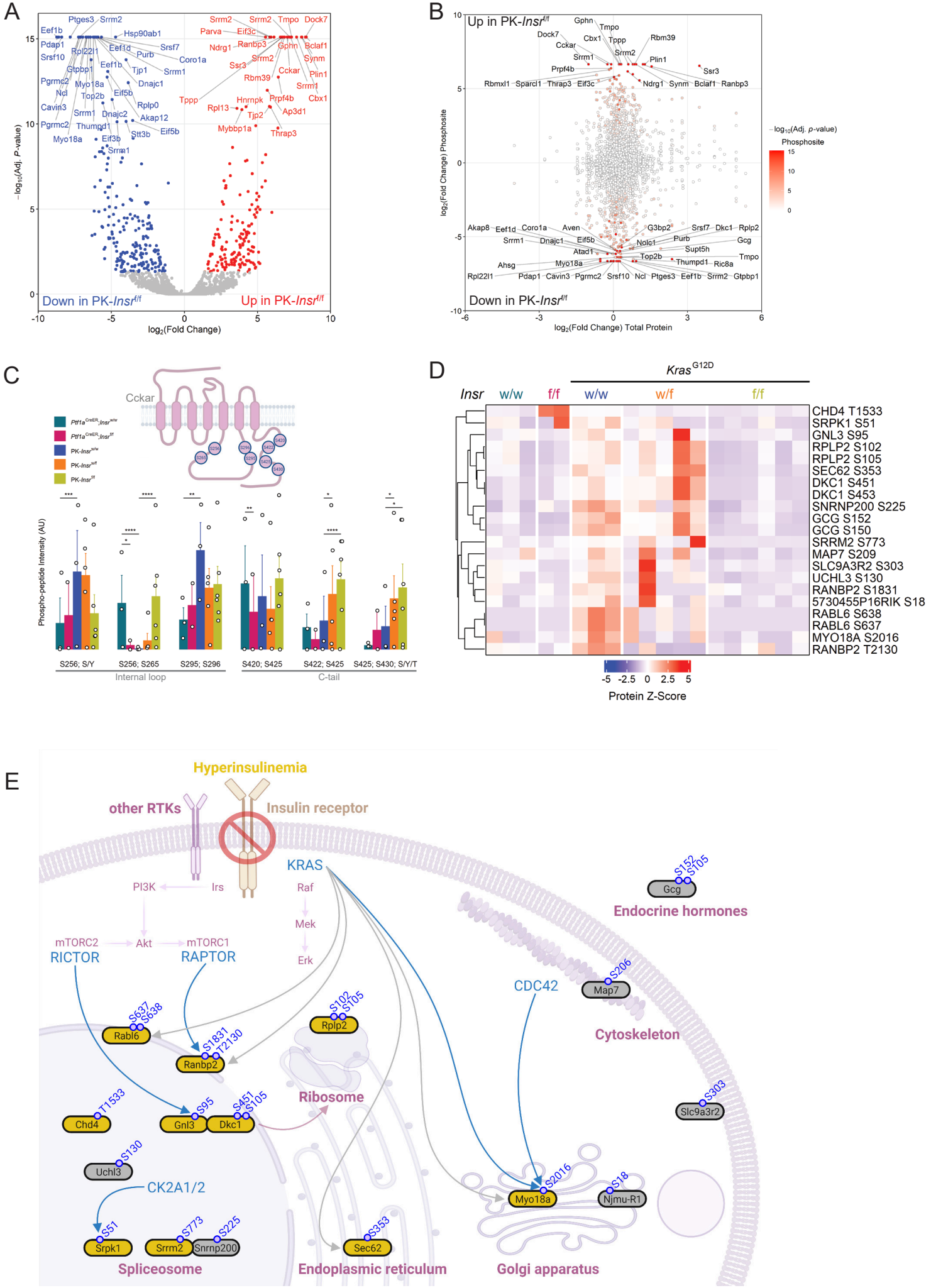
A
Down in PK-Insr f/f
Up in PK-Insr f/f
log2(Fold Change)
−log10(Adj. P-value)
B
Up in PK-Insr f/f
Down in PK-Insr f/f
log2(Fold Change) Total Protein
log2(Fold Change) Phosphosite
−log10(Adj. p-value)
Phosphosite
C
Cckar
Phospho-peptide Intensity (AU)
S256; S/Y
S256; S265
S295; S296
S420; S425
S422; S425
S425; S430; S/Y/T
Internal loop
C-tail
D
Kras G12D
Insr
w/w
f/f
w/w
w/f
f/f
CHD4 T1533
SRPK1 S51
GNL3 S95
RPLP2 S102
RPLP2 S105
SEC62 S353
DKC1 S451
DKC1 S453
SNRNP200 S225
GCG S152
GCG S150
SRRM2 S773
MAP7 S209
SLC9A3R2 S303
UCHL3 S130
RANBP2 S1831
5730455P16RIK S18
RABL6 S638
RABL6 S637
MYO18A S2016
RANBP2 T2130
Protein Z-Score
E
Hyperinsulinemia
other RTKs
Insulin receptor
KRAS
PI3K
Irs
Raf
Mek
Erk
mTORC2
RICTOR
Akt
mTORC1
RAPTOR
Endocrine hormones
Gcg
CDC42
Map7
Cytoskeleton
Rabl6
Ranbp2
Rplp2
Ribosome
Chd4
Gnl3
Dkc1
Slc9a3r2
Uchl3
CK2A1/2
Srpk1
Srrm2
Snrnp200
Spliceosome
Sec62
Endoplasmic reticulum
Myo18a
Njmu-R1
Golgi apparatus

Figure 5

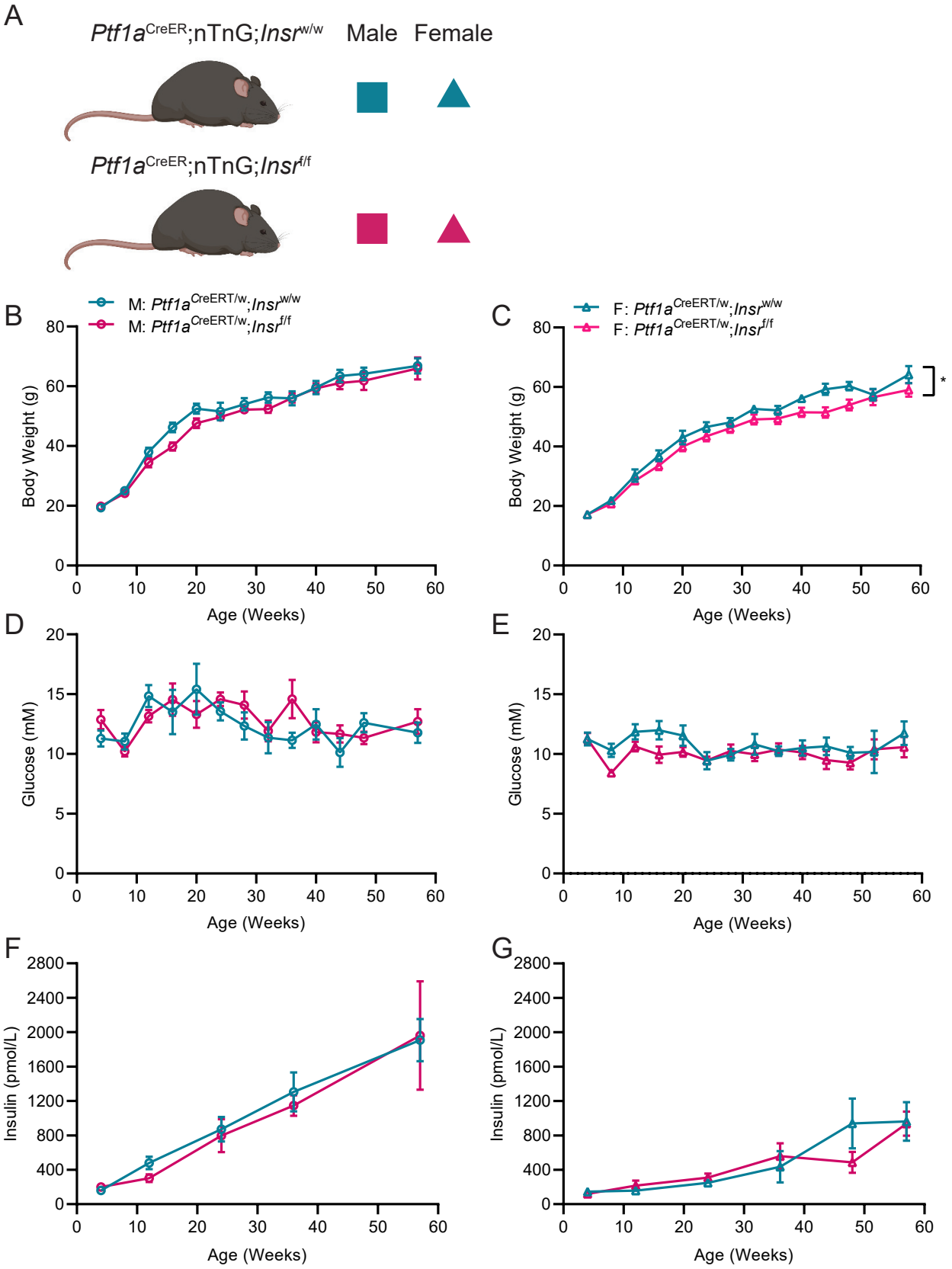

Extended Data 1

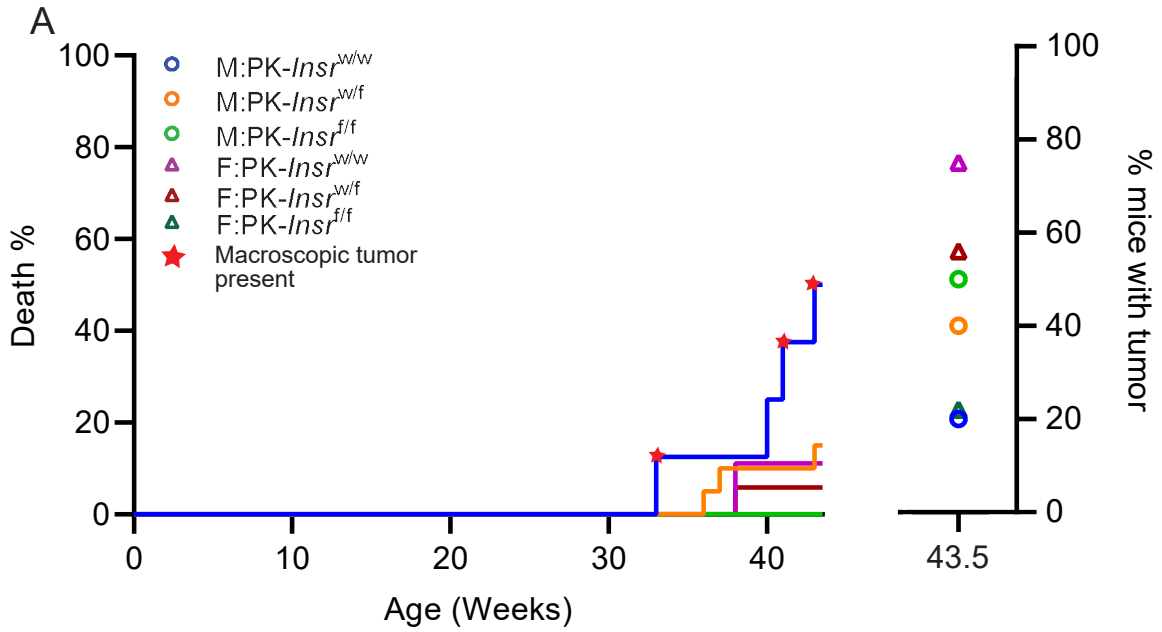
A
M:PK-Insr w/w
M:PK-Insr w/f
M:PK-Insr f/f
F:PK-Insr w/w
F:PK-Insr w/f
F:PK-Insr f/f
Macroscopic tumor present
Death %
Age (Weeks)
% mice with tumor
0
20
40
60
80
100
0
10
20
30
40
43.5

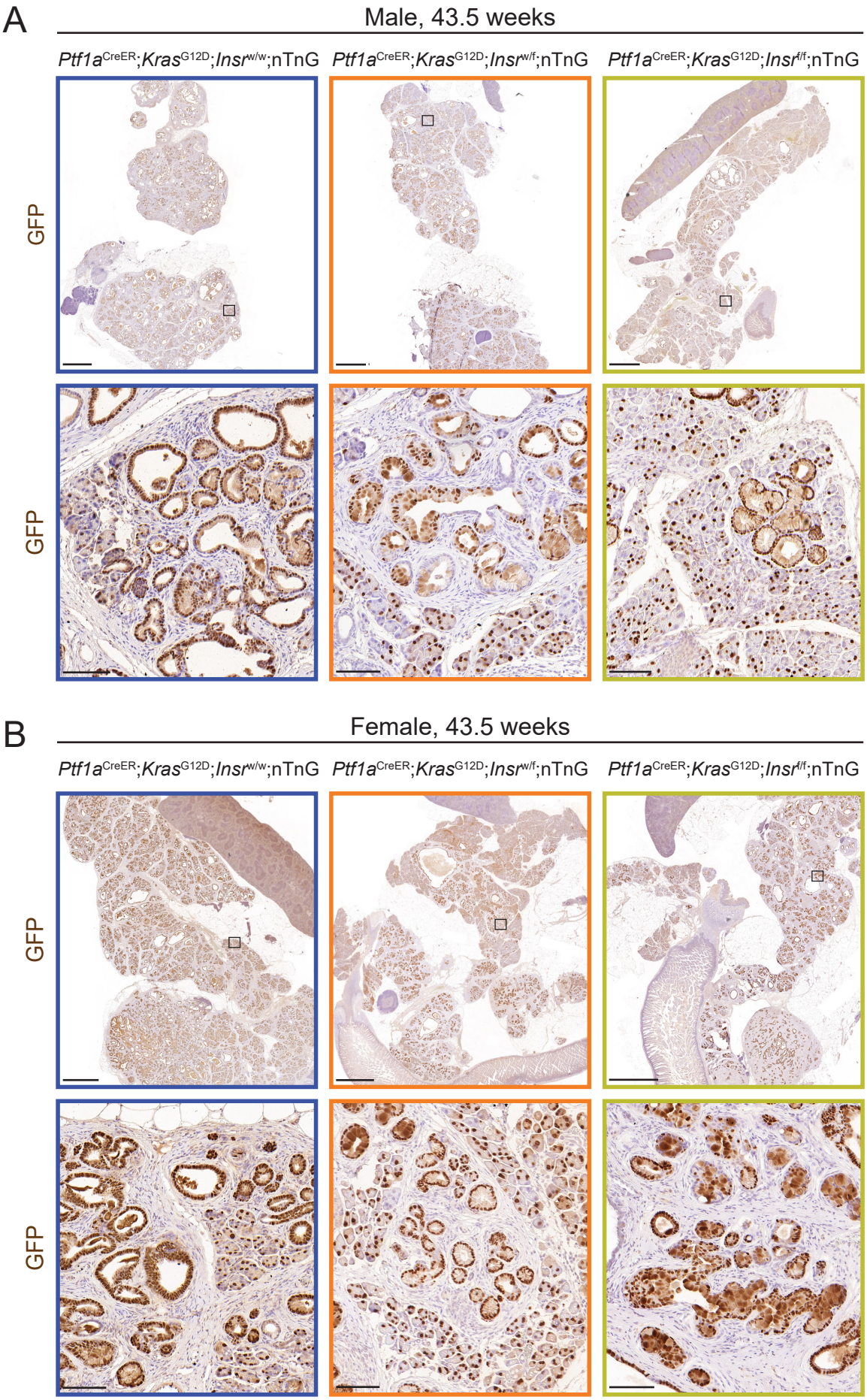
A
Male, 43.5 weeks
Ptf1aCreER;KrasG12D;Insrw/w;nTnG
Ptf1aCreER;KrasG12D;Insrw/f;nTnG
Ptf1aCreER;KrasG12D;Insrf/f;nTnG
GFP
GFP
B
Female, 43.5 weeks
Ptf1aCreER;KrasG12D;Insrw/w;nTnG
Ptf1aCreER;KrasG12D;Insrw/f;nTnG
Ptf1aCreER;KrasG12D;Insrf/f;nTnG
GFP
GFP

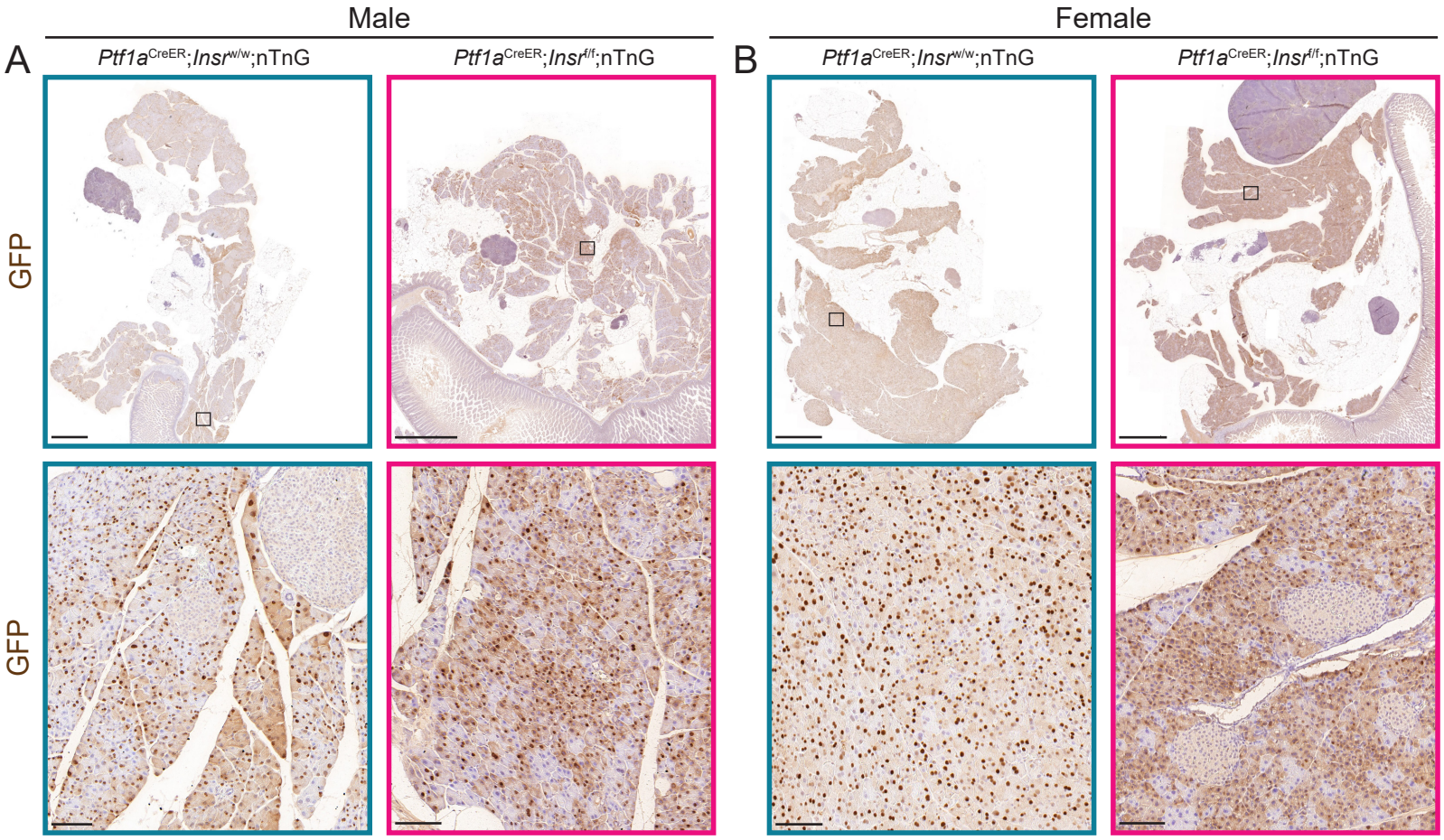

Extended Data 4

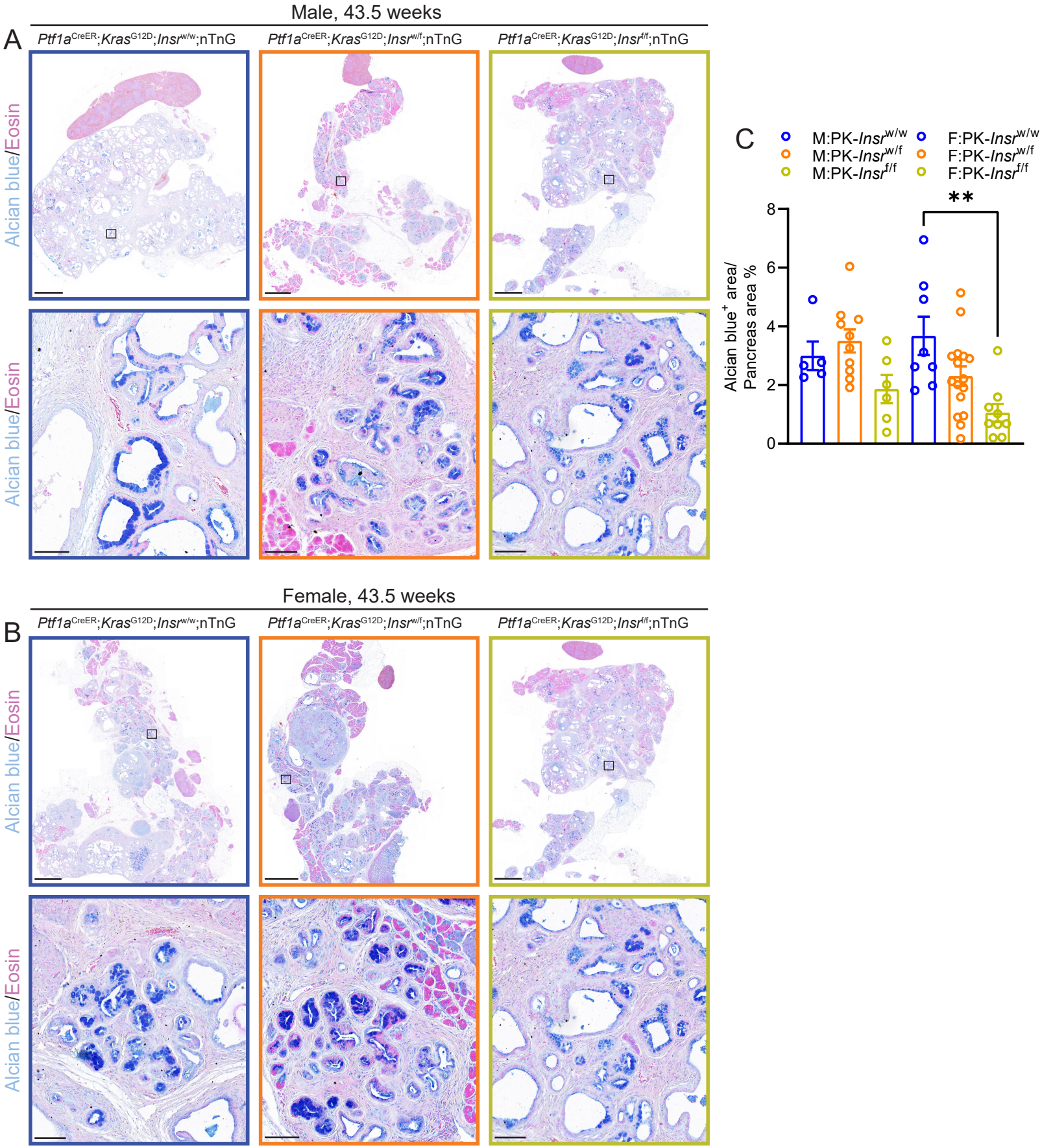

Extended Data 5

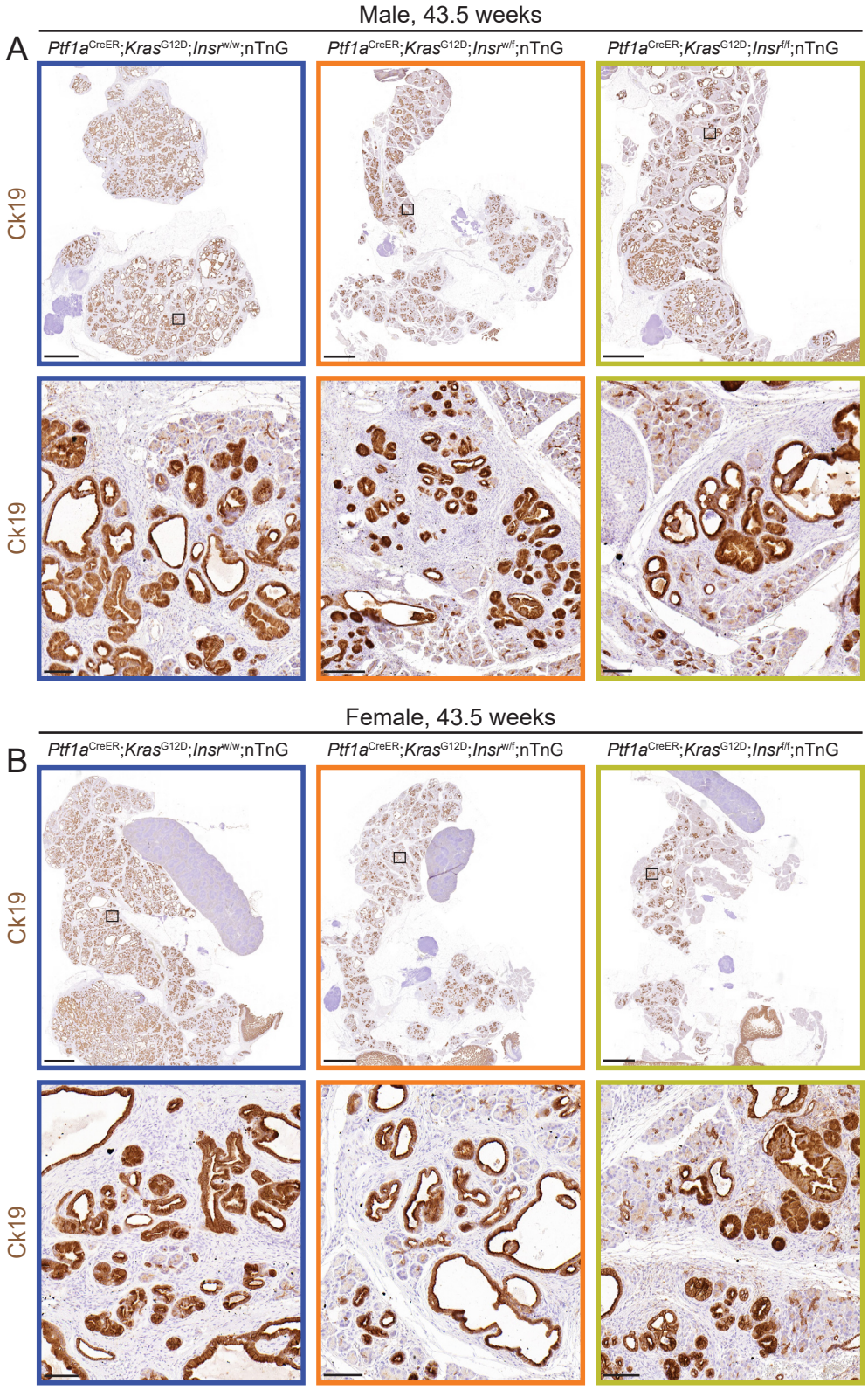
Male, 43.5 weeks
A
Ptf1aCreER;KrasG12D;Insrw/w;nTnG
Ptf1aCreER;KrasG12D;Insrw/f;nTnG
Ptf1aCreER;KrasG12D;Insrf/f;nTnG
Ck19
Ck19
Female, 43.5 weeks
B
Ptf1aCreER;KrasG12D;Insrw/w;nTnG
Ptf1aCreER;KrasG12D;Insrw/f;nTnG
Ptf1aCreER;KrasG12D;Insrf/f;nTnG
Ck19
Ck19

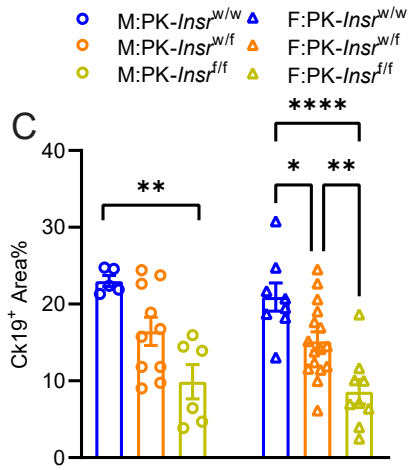
M:PK-Insrw/w
M:PK-Insrw/f
M:PK-Insrf/f
F:PK-Insrw/w
F:PK-Insrw/f
F:PK-Insrf/f
C
Ck19+ Area%
**
****
*
**

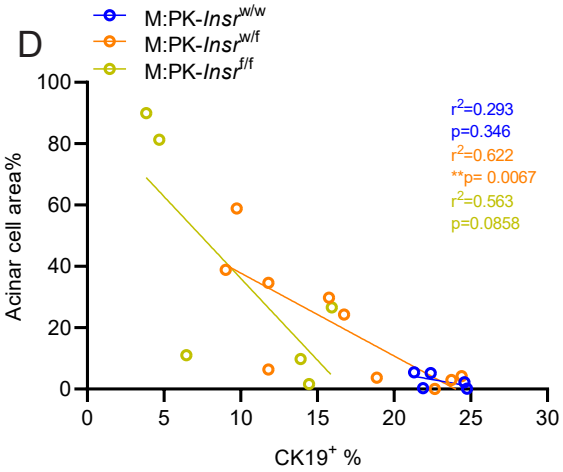
M:PK-Insrw/w
M:PK-Insrw/f
M:PK-Insrf/f
D
Acinar cell area%
CK19+ %
r2=0.293
p=0.346
r2=0.622
**p= 0.0067
r2=0.563
p=0.0858

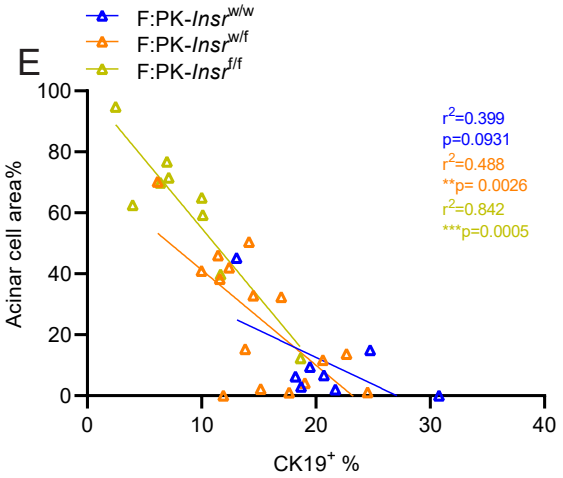
F:PK-Insrw/w
F:PK-Insrw/f
F:PK-Insrf/f
E
Acinar cell area%
CK19+ %
r2=0.399
p=0.0931
r2=0.488
**p= 0.0026
r2=0.842
***p=0.0005

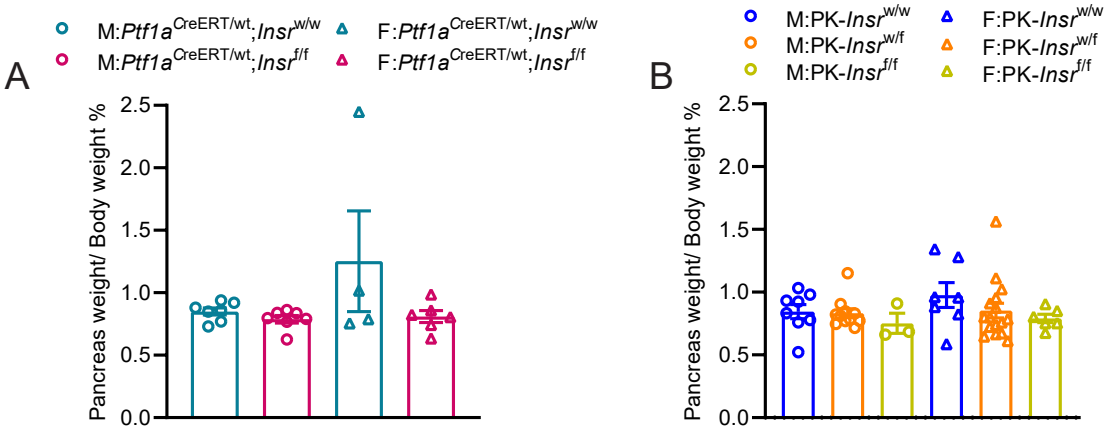
A
M:Ptf1a CreERT/wt;Insr w/w
M:Ptf1a CreERT/wt;Insr f/f
F:Ptf1a CreERT/wt;Insr w/w
F:Ptf1a CreERT/wt;Insr f/f
Pancreas weight/ Body weight %
2.5
2.0
1.5
1.0
0.5
0.0
B
M:PK-Insr w/w
M:PK-Insr w/f
M:PK-Insr f/f
F:PK-Insr w/w
F:PK-Insr w/f
F:PK-Insr f/f
Pancreas weight/ Body weight %
2.5
2.0
1.5
1.0
0.5
0.0

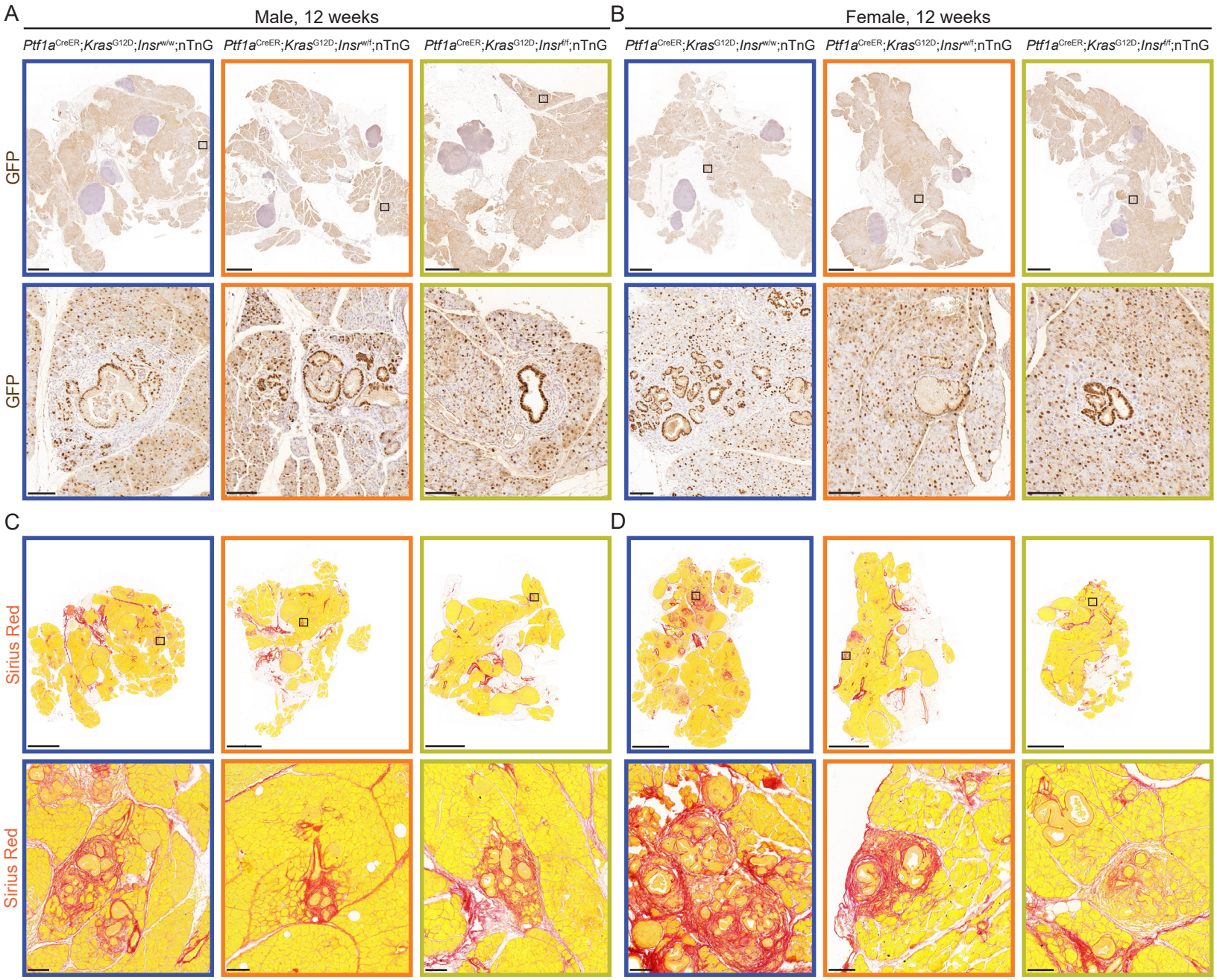

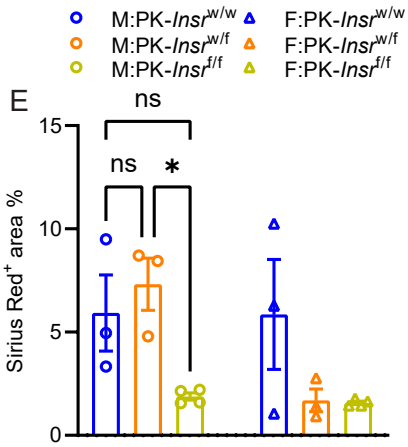

Extended Data 8

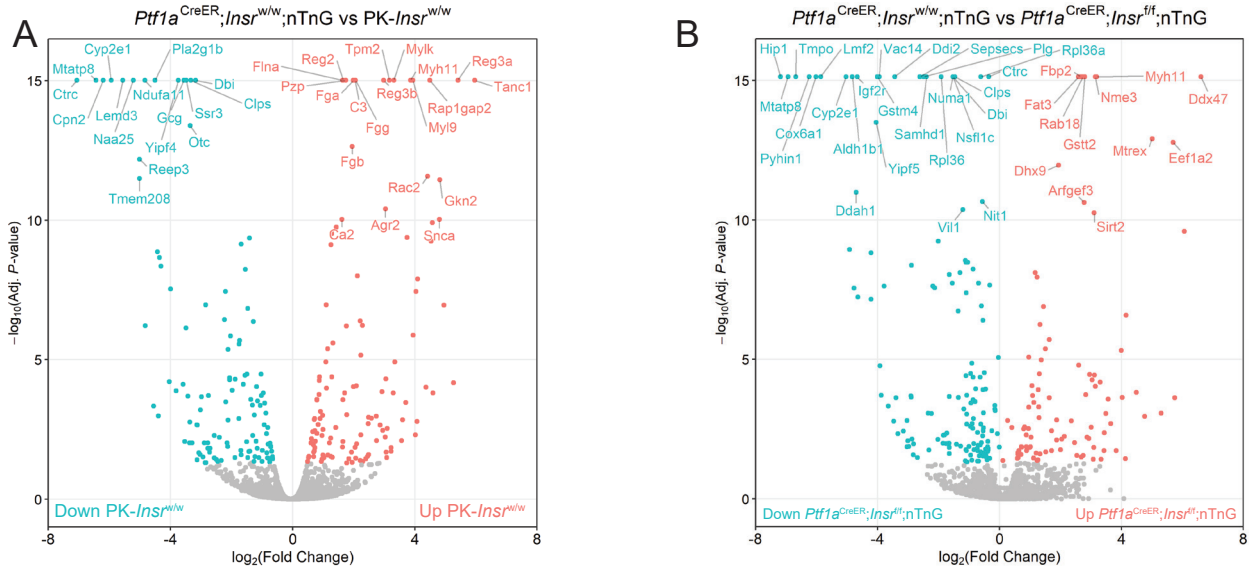

C

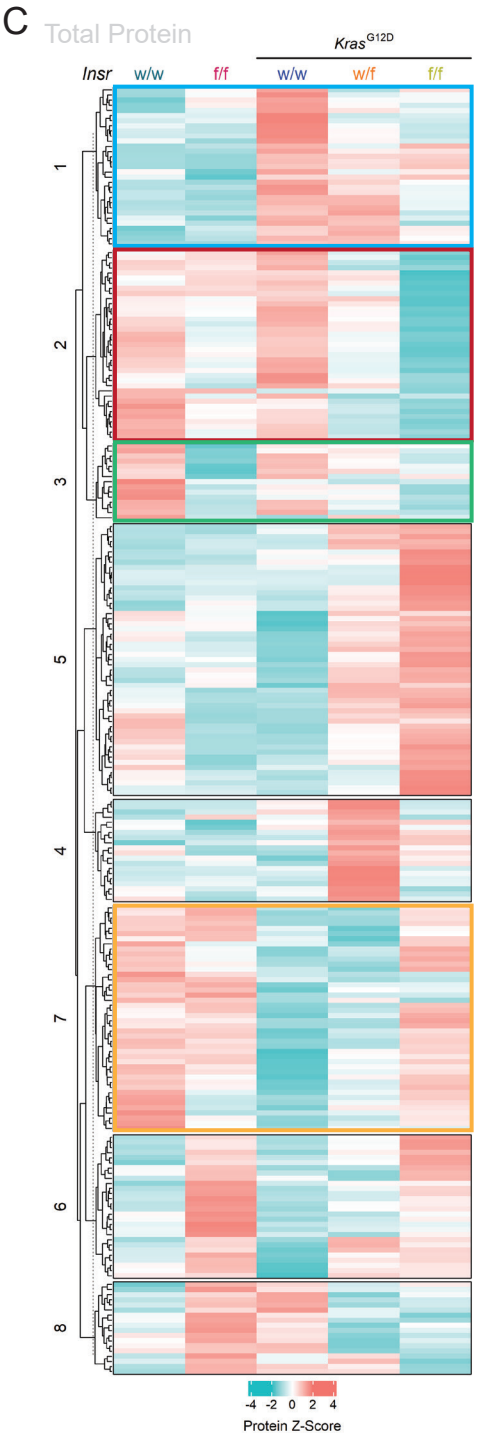

Cluster 1

Clip1
Bag3
Ctss
Rpl29
Pzp
Mzb1
Ppp4c
Fis1
Rbm26
Actr1b
Dmbt1
Tmsb10
Reg2
Fgg
Fga
Fgb
Sh3bgrl3
Pxn
Reg3a
Reg3b
Apoa2
S100a6
Igh-3
Tf
Gkn1
Tmem43
Pklr
Tagln
Mt1
Hpx
FAM120A

Cluster 2

Eif4ebp1
Snx5
Cel
Ndufa7
Cox7a2
Uqcc2
Emc10
Sycn
Pnlip
Ppih
Pnliprp2
Acly
Trmt112
Ctrb1
Pcna
Uqcrq
Afdn
Cela3b
Tcea1
Cpa1
Cpa2
Klk1
Spink1
Pnliprp1
Prss2
Cox17
Sra1
Uqcrh
Dhcr7
Srprb
Galnt6
Cela1
Cela2a
Alcam
Amy2
Cuzd1
Rnase1

Cluster 3

Atp5me
Uqcr10
Cox6c
Tbca
Rpl36
Plg
Chchd4
Clps
Ube4a
Serf2
Igf2r
Tmc4
Amy1
Kdm5a
Tmem41a

Cluster 7

Ostc
Cnbp
Ilvbl
Gna14
Rap1b
Mtnd3
Ssr3
Pla2g1b
Ubxn4
Nit1
Srp68
Rap1a
Eef2k
Dctn3
Cbs
Tmem97
Ctrc
Gcg
Stap2
Adh5
Rps24
Bzw1
Wdr77
Tpk1
Nploc4
Ube2g2
Aifm1
Lemd3
Yipf4
Ndufa11
Lonp1
mt-Co3
Snrnp200
Mtnd4
Iah1
Hm13
Nfasc
Ca3
Fabp4
Srsf5
Creb1
Ap1s1
Use1
Krt1